Energy conserving particle-in-cell methods for relativistic Vlasov–Maxwell equations of laser-plasma interaction

Yingzhe Li

Max Planck Institute for Plasma Physics, Boltzmannstrasse 2, 85748 Garching, Germany

Abstract

This work studies a class of reduced relativistic Vlasov–Maxwell equations describing laser-plasma interaction. Fully discrete schemes are obtained by discretizing distribution functions using particle-in-cell methods, discretizing electromagnetic fields with compatible finite element methods in the framework of finite element exterior calculus in space, and discrete gradient methods combined with splitting methods in time. The proposed schemes are energy conserving and discrete Poisson equations are also satisfied by the numerical solutions. Numerical experiments of parametric instability are conducted to validate the conservation properties and illustrate good long time behaviors of the numerical methods.

1 Introduction

Laser-plasma interaction is an important physical concept in the fields of inertial fusion confinement and plasma based electron accelerator schemes, which include a lot of complex physical processes when strong lasers are injected into plasmas. When the plasma density is very high and particles are accelerated by the lasers to high speeds, the relativistic and quantum effects (such as spin effects) are unignorable. There are extensive theoretical, experimental, and numerical works about laser-plasma interactions. For example, in [1] the acceleration of electrons in plasma by two counter-propagating laser pulses is discussed, and numerical simulations are done for the interactions between spin-polarized electrons beams and strong laser pulses in [31].

Kinetic equations are adopted by the laser-plasma community for theoretical and numerical explanations. As lasers usually propagate along fixed directions, the models with lower dimensions reduced from three dimensional Vlasov–Maxwell equations can be used. In this spirit, there are one and two dimensional reduced laser-plasma models proposed in the literature [5, 6], in which the reduction relies on the conservation of the canonical momentums of particles. There are a lot of existing theoretical and numerical works about these laser-plasma models, such as [7, 8, 9], in which existences of mild and global solutions are proved, also an error estimate result of a semi-Lagrangian method is given. To include spin effects, a set of kinetic equations is introduced recently and detailed in [39, 40, 41]. And in [4] a structure-preserving method for non-relativistic Vlasov–Maxwell equations with spin effects is introduced based on the geometric structures proposed in [3, 2]. In this work, we focus on the fully relativistic case.

There are mainly two classes of methods for solving kinetic models in plasma physics, the grid based methods and particle-in-cell methods [11, 12]. Grid based methods include for instances semi-Lagrangian methods [13], discontinuous Galerkin methods [10], and so on. Grid based

methods do not suffer from numerical noises, however, when the dimension of phase-space and the domain scale of simulation are very large, grid based methods are relatively costly. The particle-in-cell methods are proposed to overcome the huge computational cost. Another reason that we choose to use the particle-in-cell methods in this paper is that the spin variable is defined on a unit sphere.

Our discretizations follow the recent trend of structure-preserving methods [16, 17], which have been proposed with the purpose of preserving the intrinsic properties inherited by the given systems and thus have long term stability and accuracy. In plasma physics, some structure-preserving methods [19, 20, 21, 22, 23, 24, 25, 4, 28] have been proposed for Vlasov type equations. In these works, space discretizations are done in the framework of finite element exterior calculus [15] or discrete exterior calculus [33], after which (time-continuous) finite dimensional Poisson systems (non-canonical Hamiltonian system) are derived. From [17], we know that the only time discretization used to construct fully discrete structure-preserving methods for general non-canonical Hamiltonian systems is the so-called Hamiltonian splitting method [30, 21], which requires each Hamiltonian subsystem explicitly solvable. However, for complicated Hamiltonian systems, some subsystems can not be solved analytically. Therefore, constructing methods preserving other theoretical properties, such as energy and constraints are meaningful for long time simulations.

As for the energy-conserving methods, quadratic Hamiltonians can be conserved by the usual midpoint rule or Crank-Nicolson method. For more complicated Hamiltonians, discrete gradient methods [18] have been proposed, such as first order method in [36], second order midpoint discrete gradient [14], average vector field discrete gradient [37], and so on. All of these discrete gradients would become midpoint rules for quadratic Hamiltonians, as pointed out in [27], in which discrete gradient methods are used to construct energy conserving schemes for non-relativistic Vlasov–Maxwell equations. Another way to construct energy-conserving methods is the recently proposed so-called scalar auxiliary variable approach [26], by which an equivalent new Hamiltonian could be conserved, while the original one is not.

For relativistic Vlasov–Maxwell equations, there have already been some works about energy-conserving schemes in the literature, such as a quadratic conservative finite difference method [35]; a semi-implicit particle-in-cell method based on leap-frog and Crank-Nicolson methods [34]; a fully-implicit particle-in-cell method using implicit midpoint methods [45]; a discontinuous Galerkin method [38]; an Eulerian conservative splitting scheme [2] based on Poisson structure of the system, and so on.

In this work, two discrete gradients proposed in [36, 14] are used for the relativistic Vlasov–Maxwell equations with spin effects. The advantages of the numerical methods constructed in this work include: a) higher space accuracy can be obtained by increasing the degrees of basis functions of finite element spaces; b) both first and second order accuracy in time can be obtained; c) energies are conserved and discrete Poisson equations are satisfied by the numerical solutions as well; (d) the schemes can be extended to three dimensional case directly.

The paper is organized as follows. In section 2, one and two dimensional laser-plasma models are introduced. A Poisson bracket for the two dimensional case is proposed for the first time. In section 3, phase space discretizations are described, and finite dimensional Poisson systems with complicated (non-quadratic, non-separable) Hamiltonians are derived. In section 4, energy conserving schemes are constructed using discrete gradients and Poisson splitting methods, i.e., by splitting the Poisson matrices into several anti-symmetric parts. In section 5, two numerical experiments are conducted to validate the codes, especially conservation properties are demonstrated. Finally, we conclude this paper.

2 Laser plasma models with spin effects

In this section, we introduce the reduced fully relativistic laser-plasma models with spin effects, which are derived based on the conservation of canonical momentums of particles in one and two dimensional cases from the following three dimensional spin Vlasov–Maxwell model [4, 3].

$$\begin{aligned}
&\frac{\partial f}{\partial t}+\frac{\mathbf{p}}{\gamma}\cdot\nabla f+\left[\left(\mathbf{E}+\frac{\mathbf{p}}{\gamma}\times\mathbf{B}\right)+\mathfrak{h}\,\nabla(\mathbf{s}\cdot\mathbf{B})\right]\cdot\frac{\partial f}{\partial\mathbf{p}}+(\mathbf{s}\times\mathbf{B})\cdot\frac{\partial f}{\partial\mathbf{s}}=0,\\
&\frac{\partial\mathbf{E}}{\partial t}=\nabla\times\mathbf{B}-\int_{\mathbb{R}^6}\frac{\mathbf{p}}{\gamma}f\mathrm{d}\mathbf{p}\mathrm{d}\mathbf{s}+\mathfrak{h}\,\nabla\times\int_{\mathbb{R}^6}\mathbf{s}f\mathrm{d}\mathbf{p}\mathrm{d}\mathbf{s},\\
&\frac{\partial\mathbf{B}}{\partial t}=-\nabla\times\mathbf{E},\\
&\nabla\cdot\mathbf{E}=\int_{\mathbb{R}^6}f\mathrm{d}\mathbf{p}\mathrm{d}\mathbf{s}-1,\\
&\nabla\cdot\mathbf{B}=0,
\end{aligned}\tag{1}$$

where $f(\mathbf{x},\mathbf{p},\mathbf{s},t)$ is the distribution function of electrons, $\mathbf{x}=(x_1,x_2,x_3)^\top\in\mathbb{R}^3$ denotes position, $\mathbf{p}=(p_1,p_2,p_3)^\top\in\mathbb{R}^3$ is momentum, $\mathbf{s}=(s_1,s_2,s_3)^\top\in\mathbb{R}^3$ is the spin variable, $t\in\mathbb{R}$ is time, $\mathfrak{h}$ is the normalized Planck constant, $\mathbf{E}(\mathbf{x},t)=(E_1,E_2,E_3)^\top$ and $\mathbf{B}(\mathbf{x},t)=(B_1,B_2,B_3)^\top$ are the electro-magnetical fields, and $\gamma=\sqrt{1+|\mathbf{p}|^2}$ is the relativistic factor. The Vlasov–Maxwell system with spin effects (1) is a Hamiltonian system [3] with the Hamiltonian

$$\mathcal{H}=\int(\sqrt{1+|\mathbf{p}|^2}-1)f\mathrm{d}\mathbf{x}\mathrm{d}\mathbf{p}\mathrm{d}\mathbf{s}+\frac{1}{2}\int|\mathbf{E}|^2\mathrm{d}\mathbf{x}+\frac{1}{2}\int|\mathbf{B}|^2\mathrm{d}\mathbf{x}+\mathfrak{h}\int\mathbf{s}\cdot\mathbf{B}f\mathrm{d}\mathbf{x}\mathrm{d}\mathbf{p}\mathrm{d}\mathbf{s}.\tag{2}$$

2.1 One dimensional case

We assume that an electromagnetic wave is propagating in the longitudinal x_1 direction and that all unknowns only depend on x_1 spatially. The longitudinal variable (x_1,p_1) will be simply denoted by (x,p) for convenience in this subsection. Choosing the Coulomb gauge $\nabla\cdot\mathbf{A}=0$, the vector potential $\mathbf{A}$ can be denoted as $\mathbf{A}=(0,A_2,A_3)=:(0,\mathbf{A}_\perp)$. Using $\mathbf{E}=-\nabla\phi-\partial_t\mathbf{A}$ with ϕ the scalar potential, and denoting $\mathbf{E}=(E_1,E_2,E_3)=:(E_1,\mathbf{E}_\perp)$, we then obtain $\mathbf{E}_\perp=-\partial_t\mathbf{A}_\perp$ and $E_1=-\partial_x\phi$. As the system only depends on x_1 in space, we know that the second and third components of canonical momentum $\mathbf{p}+\mathbf{A}$ are conserved by particles' equations, i.e., p_2+A_2, p_3+A_3 are both constants for each particle. Assuming $p_2=-A_2$, $p_3=-A_3$, we obtain the following reduced one dimensional (1D) model,

$$\begin{aligned}
&\frac{\partial f}{\partial t}+\frac{p}{\gamma}\frac{\partial f}{\partial x}+\left[E_1-\frac{\mathbf{A}_\perp}{\gamma}\cdot\frac{\partial\mathbf{A}_\perp}{\partial x}+\mathfrak{h}\nabla(\mathbf{s}\cdot\mathbf{B})\right]\frac{\partial f}{\partial p}+(\mathbf{s}\times\mathbf{B})\cdot\frac{\partial f}{\partial\mathbf{s}}=0,\\
&\frac{\partial E_1}{\partial t}=-\int_{\mathbb{R}^4}\frac{p}{\gamma}f\mathrm{d}p\mathrm{d}\mathbf{s},\\
&\frac{\partial E_2}{\partial t}=-\frac{\partial^2A_2}{\partial x^2}+A_2\int_{\mathbb{R}^4}\frac{f}{\gamma}\mathrm{d}p\mathrm{d}\mathbf{s}-\mathfrak{h}\int_{\mathbb{R}^4}s_3\frac{\partial f}{\partial x}\mathrm{d}p\mathrm{d}\mathbf{s},\\
&\frac{\partial E_3}{\partial t}=-\frac{\partial^2A_3}{\partial x^2}+A_3\int_{\mathbb{R}^4}\frac{f}{\gamma}\mathrm{d}p\mathrm{d}\mathbf{s}+\mathfrak{h}\int_{\mathbb{R}^4}s_2\frac{\partial f}{\partial x}\mathrm{d}p\mathrm{d}\mathbf{s},\\
&\frac{\partial\mathbf{A}_\perp}{\partial t}=-\mathbf{E}_\perp,\\
&\frac{\partial E_1}{\partial x}=\int_{\mathbb{R}^4}f\mathrm{d}p\mathrm{d}\mathbf{s}-1,\quad\text{(Poisson equation)},
\end{aligned}\tag{3}$$

where $f(x,p,\mathbf{s},t)$ is the distribution function, relativistic factor γ is a function depending on p and $\mathbf{A}_\perp(x)$ as $\gamma(p,\mathbf{A}_\perp(x)) = \sqrt{1+p^2+|\mathbf{A}_\perp|^2}$, and $\mathbf{B} = \nabla\times\mathbf{A} = \left(0, -\frac{\partial A_3}{\partial x}, \frac{\partial A_2}{\partial x}\right)^\top$. We can see that γ depends on both x and p, and is non-separable, which bring some difficulties for constructing energy-conserving schemes. This reduced spin Vlasov–Maxwell system (3) possesses a non-canonical Poisson structure [4]. For any two functionals $\mathcal{F}$ and $\mathcal{G}$ depending on the unknowns $f, \mathbf{E}$, and $\mathbf{A}_\perp$, the Poisson bracket is

$$\begin{aligned}\{\mathcal{F},\mathcal{G}\} = &\int_{\mathbb{R}^5} f\left[\frac{\delta\mathcal{F}}{\delta f}, \frac{\delta\mathcal{G}}{\delta f}\right]_{xp} \mathrm{d}x\mathrm{d}p\mathrm{d}\mathbf{s} + \int_{\mathbb{R}^5}\left(\frac{\delta\mathcal{F}}{\delta E_1}\frac{\partial f}{\partial p}\frac{\delta\mathcal{G}}{\delta f} - \frac{\delta\mathcal{G}}{\delta E_1}\frac{\partial f}{\partial p}\frac{\delta\mathcal{F}}{\delta f}\right)\mathrm{d}x\mathrm{d}p\mathrm{d}\mathbf{s}\\ &+\int_{\mathbb{R}}\left(\frac{\delta\mathcal{G}}{\delta\mathbf{A}_\perp}\cdot\frac{\delta\mathcal{F}}{\delta\mathbf{E}_\perp} - \frac{\delta\mathcal{F}}{\delta\mathbf{A}_\perp}\cdot\frac{\delta\mathcal{G}}{\delta\mathbf{E}_\perp}\right)\mathrm{d}x + \frac{1}{\mathfrak{h}}\int_{\mathbb{R}^5} f\mathbf{s}\cdot\left(\frac{\partial}{\partial\mathbf{s}}\frac{\delta\mathcal{F}}{\delta f}\times\frac{\partial}{\partial\mathbf{s}}\frac{\delta\mathcal{G}}{\delta f}\right)\mathrm{d}x\mathrm{d}p\mathrm{d}\mathbf{s},\end{aligned} \tag{4}$$

where $[h,g]_{xp} = \partial_x h\partial_p g - \partial_x g\partial_p h$. The Hamiltonian functional, which is the sum of kinetic, electric, magnetic and Zeeman (spin-dependent) energies, is

$$\begin{aligned}\mathcal{H}(f,\mathbf{E},\mathbf{A}_\perp) = &\int_{\mathbb{R}^5}(\sqrt{1+p^2+|\mathbf{A}_\perp|^2}-1)f\mathrm{d}x\mathrm{d}p\mathrm{d}\mathbf{s} + \frac{1}{2}\int_{\mathbb{R}}|\mathbf{E}|^2\mathrm{d}x\\ &+\frac{1}{2}\int_{\mathbb{R}}\left|\frac{\partial\mathbf{A}_\perp}{\partial x}\right|^2\mathrm{d}x + \mathfrak{h}\int_{\mathbb{R}^5}\left(-s_2\frac{\partial A_3}{\partial x}+s_3\frac{\partial A_2}{\partial x}\right)f\mathrm{d}x\mathrm{d}p\mathrm{d}\mathbf{s}.\end{aligned} \tag{5}$$

Then the reduced spin Vlasov-Maxwell system of equations (3) can be reformulated as

$$\frac{\partial\mathcal{Z}}{\partial t} = \{\mathcal{Z},\mathcal{H}\},$$

where $\mathcal{Z} = (f, E_1, E_2, E_3, A_2, A_3)$. For the 1D model (3), periodic boundary condition for x in a finite domain and vanishing boundary conditions for $p\in\mathbb{R}$ and $\mathbf{s}\in\mathbb{R}^3$ are considered. Initial condition is $\mathcal{Z}(t=0) = \mathcal{Z}_0 = (f_0, \mathbf{E}_0, \mathbf{A}_{\perp,0})$.

2.2 Two dimensional case

Similar to the one dimensional reduction, we consider an electromagnetic wave propagating in the longitudinal x_1, x_2 direction and the system only depends on x_1, x_2 spatially, then $p_3 + A_3$ is conserved for each particle. Assuming $p_3 = -A_3$ and combining with two dimensional reduced

Maxwell's equations, we have the following reduced two dimensional (2D) model,

$$
\begin{aligned}
&\frac{\partial f}{\partial t}+\frac{\mathbf{p}}{\gamma}\cdot\frac{\partial f}{\partial \mathbf{x}}+\left(\mathbf{E}_{12}+\tilde{\mathbf{F}}+\mathfrak{h}\nabla(\mathbf{s}\cdot\mathbf{B})\right)\cdot\frac{\partial f}{\partial \mathbf{p}}+(\mathbf{s}\times\mathbf{B})\cdot\frac{\partial f}{\partial \mathbf{s}}=0,\\
&\mathbf{B}=\left(\frac{\partial A_3}{\partial x_2},-\frac{\partial A_3}{\partial x_1},B_3\right)^\top,\quad \tilde{\mathbf{F}}=\left(\frac{p_2B_3+A_3B_2}{\gamma},-\frac{p_1B_3+A_3B_1}{\gamma}\right)^\top\\
&\frac{\partial E_1}{\partial t}=\frac{\partial B_3}{\partial 2}-\int\frac{p_1}{\gamma}f\mathrm{d}\mathbf{p}\mathrm{d}\mathbf{x}+\mathfrak{h}\int s_3\frac{\partial f}{\partial x_2}\mathrm{d}\mathbf{p}\mathrm{d}\mathbf{s},\\
&\frac{\partial E_2}{\partial t}=-\frac{\partial B_3}{\partial x}-\int\frac{p_2}{\gamma}f\mathrm{d}\mathbf{p}\mathrm{d}\mathbf{x}-\mathfrak{h}\int s_3\frac{\partial f}{\partial x_1}\mathrm{d}\mathbf{p}\mathrm{d}\mathbf{s},\\
&\frac{\partial B_3}{\partial t}=\frac{\partial E_1}{\partial x_2}-\frac{\partial E_2}{\partial x_1},\\
&\frac{\partial A_3}{\partial t}=-E_3,\\
&\frac{\partial E_3}{\partial t}=-\frac{\partial^2 A_3}{\partial x_1^2}-\frac{\partial^2 A_3}{\partial x_2^2}+\int\frac{A_3}{\gamma}f\mathrm{d}\mathbf{p}\mathrm{d}\mathbf{x}+\mathfrak{h}\int\left(s_2\frac{\partial f}{\partial x_1}-s_1\frac{\partial f}{\partial x_2}\right)\mathrm{d}\mathbf{p}\mathrm{d}\mathbf{s},\\
&\nabla_{\mathbf{x}}\cdot\mathbf{E}_{12}=\int f\mathrm{d}\mathbf{p}\mathrm{d}\mathbf{s}-1,\quad\text{(Poisson equation)},
\end{aligned}
\tag{6}
$$

where $f(\mathbf{x},\mathbf{p},\mathbf{s},t)$ is the distribution function , $\mathbf{x}=(x_1,x_2)^\top,\mathbf{p}=(p_1,p_2)^\top$, $\mathbf{s}\in\mathbb{R}^3$, $\mathbf{E}_{12}=(E_1,E_2)^\top$, and γ is a function depending on $\mathbf{p}$ and $A_3(\mathbf{x})$ as $\gamma(\mathbf{p},A_3(\mathbf{x}))=\sqrt{1+|\mathbf{p}|^2+|A_3|^2}$. For the above model, we propose its Poisson bracket as

$$
\begin{aligned}
\{\mathcal{F},\mathcal{G}\}(f(\mathbf{x},\mathbf{p}),A_3,B_3,\mathbf{E})&=\int f\left[\frac{\delta\mathcal{F}}{\delta f},\frac{\delta\mathcal{G}}{\delta f}\right]_{\mathbf{xp}}\mathrm{d}\mathbf{x}\mathrm{d}\mathbf{p}+\int\frac{\delta\mathcal{G}}{\delta B_3}\nabla\times\frac{\delta\mathcal{F}}{\delta\mathbf{E}_{12}}-\frac{\delta\mathcal{F}}{\delta B_3}\nabla\times\frac{\delta\mathcal{G}}{\delta\mathbf{E}_{12}}\mathrm{d}\mathbf{x}\mathrm{d}\mathbf{p}\\
&+\int\left(\frac{\delta\mathcal{F}}{\delta E_3}\frac{\delta\mathcal{G}}{\delta A_3}-\frac{\delta\mathcal{G}}{\delta E_3}\frac{\delta\mathcal{F}}{\delta A_3}\right)\mathrm{d}\mathbf{x}+\int f\left(\frac{\partial}{\partial\mathbf{p}}\frac{\delta\mathcal{F}}{\delta f}\cdot\frac{\delta\mathcal{G}}{\delta\mathbf{E}_{12}}-\frac{\partial}{\partial\mathbf{p}}\frac{\delta\mathcal{G}}{\delta f}\cdot\frac{\delta\mathcal{F}}{\delta\mathbf{E}_{12}}\right)\mathrm{d}\mathbf{x}\mathrm{d}\mathbf{p}\\
&+\int fB_3\left(\frac{\partial}{\partial p_1}\frac{\delta\mathcal{F}}{\delta f}\frac{\partial}{\partial p_2}\frac{\delta\mathcal{G}}{\delta f}-\frac{\partial}{\partial p_2}\frac{\delta\mathcal{F}}{\delta f}\frac{\partial}{\partial p_1}\frac{\delta\mathcal{G}}{\delta f}\right)\mathrm{d}\mathbf{x}\mathrm{d}\mathbf{p}+\frac{1}{\mathfrak{h}}\int_{\mathbb{R}^5}f\mathbf{s}\cdot\left(\frac{\partial}{\partial\mathbf{s}}\frac{\delta\mathcal{F}}{\delta f}\times\frac{\partial}{\partial\mathbf{s}}\frac{\delta\mathcal{G}}{\delta f}\right)\mathrm{d}\mathbf{s}\mathrm{d}\mathbf{p}\mathrm{d}\mathbf{x},
\end{aligned}
\tag{7}
$$

where $[h,g]_{\mathbf{xp}}=\nabla_{\mathbf{x}}h\cdot\nabla_{\mathbf{p}}g-\nabla_{\mathbf{x}}g\cdot\nabla_{\mathbf{p}}h$. With the following Hamiltonian,

$$
\begin{aligned}
\mathcal{H}=&\int\left(\sqrt{1+|\mathbf{p}|^2+|A_3|^2}-1\right)f\mathrm{d}\mathbf{s}\mathrm{d}\mathbf{p}\mathrm{d}\mathbf{x}+\mathfrak{h}\int\mathbf{s}\cdot\mathbf{B}f\mathrm{d}\mathbf{s}\mathrm{d}\mathbf{p}\mathrm{d}\mathbf{x},\\
&+\frac{1}{2}\int|\mathbf{E}|^2\mathrm{d}\mathbf{x}+\frac{1}{2}\int|\nabla^\top A_3|^2\mathrm{d}\mathbf{x}+\frac{1}{2}\int B_3^2\mathrm{d}\mathbf{x},
\end{aligned}
\tag{8}
$$

the above 2D model (6) could be written as

$$
\frac{\partial\mathcal{Z}}{\partial t}=\{\mathcal{Z},\mathcal{H}\},
$$

where $\mathcal{Z}=(f,\mathbf{E},A_3,B_3)$. In the above equations, operators $\nabla,\nabla^\top,\nabla\times$ are defined as

$$
\nabla f=(\partial_{x_1}f,\partial_{x_2}f)^\top,\nabla^\top f=(\partial_{x_2}f,-\partial_{x_1}f)^\top,\nabla\times\mathbf{f}=\partial_{x_1}f_2-\partial_{x_2}f_1.
$$

Similar to 1D model (3), periodic boundary condition for $\mathbf{x}$ in a finite domain and vanishing boundary conditions for $\mathbf{p}\in\mathbb{R}^2$ and $\mathbf{s}\in\mathbb{R}^3$ are considered. Initial condition is $\mathcal{Z}(t=0)=\mathcal{Z}_0=(f_0,\mathbf{E}_0,A_{3,0},B_{3,0})$.

3 Semi-discretization

In this section, we introduce the phase-space discretizations for the above two reduced models (3) and (6) in the framework of finite element exterior calculus [15] and particle-in-cell methods, after which two finite dimensional Hamiltonian systems are obtained.

3.1 One dimensional case

Following [23, 4, 32], we discretize the components of the electromagnetic fields differently. Specifically we consider E_2, E_3, A_2, A_3 as 0-forms and E_1, B_2, B_3 as 1-forms, which are discretized in finite element spaces $V_0 \subset H^1$ and $V_1 \subset L^2$, respectively. There exists a commuting diagram (9) for the involved functional spaces in one dimensional case, between continuous spaces in the upper line and discrete subspaces in the lower line. The projectors Π_0 and Π_1 must be constructed or chosen carefully in order to assure the diagram to be commuting, such as the quasi-inter/histopolation detailed in [32].

$$\begin{array}{ccc} H^1 & \xrightarrow{\frac{\mathrm{d}}{\mathrm{d}x}} & L^2 \\ \Big\downarrow{\scriptstyle \Pi_0} & & \Big\downarrow{\scriptstyle \Pi_1} \\ V_0 & \xrightarrow{\frac{\mathrm{d}}{\mathrm{d}x}} & V_1 \end{array} \tag{9}$$

In the following, the basis functions of B-splines [29] with periodic boundary condition are presented, readers could refer to [32, 24] for the cases with other boundary conditions. The knot vector $\{x_i\}_{0\leq i\leq M+2p}$ is generated from a uniform partition of the domain $[0, L]$ into M parts of equal length $\Delta x = L/M$ and periodic extension at the boundaries:

$$\{x_i\}_{0\leq i\leq M+2p} = \{\underbrace{-q\Delta x, \cdots, -\Delta x}_{q \text{ terms}}, \underbrace{0, \Delta x, 2\Delta x, \cdots, L-\Delta x, L}_{M+1 \text{ terms}}, \underbrace{L+\Delta x, \cdots, L+q\Delta x}_{q \text{ terms}}\}. \tag{10}$$

The i-th B-spline N_i^q of degree q is then recursively defined by

$$N_i^q(x) := w_i^q(x) N_i^{q-1}(x) + (1 - w_{i+1}^p(x)) N_{i+1}^{q-1}(x), \quad w_i^q(x) = \frac{x - x_i}{x_{i+q} - x_i},$$
$$N_i^0(x) := \begin{cases} 1, & x \in [x_i, x_{i+1}), \\ 0, & \text{else}, \end{cases}$$

and we can find that the support of N_i^q is $[x_i, \cdots, x_{i+q+1})$. An important property of B-splines is that derivative of a B-spline is given by

$$\frac{\mathrm{d}N_i^q}{\mathrm{d}x} = \frac{q}{x_{i+q} - x_i} N_i^{q-1} - \frac{q}{x_{i+q+1} - x_{i+1}} N_{i+1}^{q-1} := D_{i-1}^{q-1} - D_i^{q-1},$$

where D_i^{q-1} is the i-th D spline of degree $q-1$.

The basis functions of V_0, V_1 are chosen as

$$\mathbf{\Lambda}^0 = (N_0^q, \cdots, N_{n_N-1}^q)^\top, \quad \mathbf{\Lambda}^1 = (D_0^q, \cdots, D_{n_D-1}^q)^\top,$$

where n_N and n_D denote the number of distinct B-splines and D-splines respectively. Note that $D_{-1}^{q-1} = D_{M+q-1}^{q-1} = 0$ on $[0, L]$ from the definition of D_i^{q-1}, so we remove these two splines from the space of D-splines. In case of periodic splines, the last q (resp. $q-1$ in case of the D-splines)

splines are the same as the first q (resp. $q-1$) splines. Thus ignoring the last q (resp. $q-1$ in case of the D-splines), we have

$$n_N = M, \quad n_D = n_N.$$

It is worth to mention that for other boundary condition cases $n_N \neq n_D$ as detailed in [32]. From the definition of $\mathbf{\Lambda}^0$ and $\mathbf{\Lambda}^1$, it is followed that

$$\frac{\mathrm{d}}{\mathrm{d}x}(\mathbf{\Lambda}^0)^\top = (\mathbf{\Lambda}^1)^\top \mathbb{G}, \quad \mathbb{G} \in \mathbb{R}^{n_D \times n_N},$$

where $\mathbb{G}$ is the matrix corresponding to the derivative operator.

The approximations of components of the electric field and magnetic potential are [43, 23]

$$E_{1,h}(t,x) = \sum_{j=0}^{n_D-1} e_{1,j}(t) D_j^{q-1}(x) = (\mathbf{\Lambda}^1)^\top \mathbf{e}_1, \; E_{i,h}(t,x) = \sum_{j=0}^{n_N-1} e_{i,j}(t) N_j^p(x) = (\mathbf{\Lambda}^0)^\top \mathbf{e}_i, \; i \in \{2,3\},$$

$$A_{i,h}(t,x) = \sum_{j=0}^{n_N-1} a_{i,j}(t) N_j^p(x) = (\mathbf{\Lambda}^0)^\top \mathbf{a}_i, \quad i \in \{2,3\}.$$

Recall that $\mathbf{E}_\perp = (E_2, E_3)^\top$ and $\mathbf{A}_\perp = (A_2, A_3)^\top$, then

$$\mathbf{E}_{\perp,h}(t,x) = (\mathbf{\Lambda}^0)^\top \mathbf{e}_2 \hat{\mathbf{e}}_1 + (\mathbf{\Lambda}^0)^\top \mathbf{e}_3 \hat{\mathbf{e}}_2, \quad \mathbf{A}_{\perp,h}(t,x) = (\mathbf{\Lambda}^0)^\top \mathbf{a}_2 \hat{\mathbf{e}}_1 + (\mathbf{\Lambda}^0)^\top \mathbf{a}_3 \hat{\mathbf{e}}_2,$$

where $\hat{\mathbf{e}}_\mu$ is the unit vector in x_μ direction, $\mu \in \{1,2\}$.

The distribution function $f(t,x,p,\mathbf{s})$ is discretized as the sum of finite number of particles with constant weights, i.e.,

$$f(t,x,p,\mathbf{s}) \approx f_h(t,x,p,\mathbf{s}) = \sum_{a=0}^{N_p-1} \omega_a \delta(x - x_a(t)) \delta(p - p_a(t)) \delta(\mathbf{s} - \mathbf{s}_a(t)), \tag{11}$$

where N_p is the total particle number, ω_a, x_a, p_a, and $\mathbf{s}_a$ denote the weight, the position, the momentum, and the spin coordinates of a-th ($0 \leq a < N_p$) particle, respectively.

We introduce the following vectors and matrices before the presentations of discrete Poisson bracket and Hamiltonian.

$$\begin{aligned}
&\mathbf{X} := (x_0, \cdots, x_{N_p-1})^\top \in \mathbb{R}^{N_p}, \quad \mathbf{P} := (p_0, \cdots, p_{N_p-1})^\top \in \mathbb{R}^{N_p}, \\
&\mathbf{S}_i := (s_{0,i}, \cdots, s_{N_p-1,i})^\top, \quad i \in \{1,2,3\} && \in \mathbb{R}^{N_p}, \\
&\mathbf{S} := (s_{0,1}, s_{0,2}, s_{0,3}, \cdots, s_{N_p-1,1}, s_{N_p-1,2}, s_{N_p-1,3})^\top && \in \mathbb{R}^{3N_p}, \\
&\mathbb{\Lambda}_0(\mathbf{X}) := (N_i^p(x_a))_{0 \leq a < N_p, 0 \leq i < n_N} && \in \mathbb{R}^{N_p \times n_N}, \\
&\mathbb{\Lambda}_1(\mathbf{X}) := (D_i^{q-1}(x_a))_{0 \leq a < N_p, 0 \leq i < n_D} && \in \mathbb{R}^{N_p \times n_D}, \\
&\mathbb{W} := \mathrm{diag}(\omega_0, \cdots, \omega_{N_p-1}) && \in \mathbb{R}^{N_p \times N_p},
\end{aligned}$$

$$\mathbb{S} := \mathrm{diag}(\mathbb{S}_0, \cdots, \mathbb{S}_{N_p-1}) \in \mathbb{R}^{3N_p \times 3N_p}, \quad \mathbb{S}_a := \frac{1}{\omega_a} \begin{pmatrix} 0 & s_{a,3} & -s_{a,2} \\ -s_{a,3} & 0 & s_{a,1} \\ s_{a,2} & -s_{a,1} & 0 \end{pmatrix},$$

$$\mathbb{M}_0 := \int_0^L \mathbf{\Lambda}^0(x)(\mathbf{\Lambda}^0(x))^\top \mathrm{d}x \in \mathbb{R}^{n_N \times n_N}, \quad \mathbb{M}_1 := \int_0^L \mathbf{\Lambda}^1(x)(\mathbf{\Lambda}^1(x))^\top \mathrm{d}x \in \mathbb{R}^{n_D \times n_D}. \tag{12}$$

$\mathbb{M}_0, \mathbb{M}_1$ are called mass matrices of V_0, V_1, respectively. By discretizing the Poisson bracket (4) using discrete functional derivatives as in [4], we have the following discrete Poisson bracket.

$$\{F, G\} = (\nabla_{\mathbf{u}} F)^\top \mathbb{J}(\mathbf{u}) \nabla_{\mathbf{u}} G, \tag{13}$$

where $\mathbf{u} = (\mathbf{X}^\top, \mathbf{P}^\top, \mathbf{S}^\top, \mathbf{e}_x^\top, \mathbf{e}_y^\top, \mathbf{e}_z^\top, \mathbf{a}_y^\top, \mathbf{a}_z^\top)^\top$ and the matrix $\mathbb{J}(\mathbf{u})$ is defined by

$$\mathbb{J}(\mathbf{u}) = \begin{pmatrix} \mathbf{0} & \mathbb{W}^{-1} & \mathbf{0} & \mathbf{0} & \mathbf{0} & \mathbf{0} & \mathbf{0} & \mathbf{0} \\ -\mathbb{W}^{-1} & \mathbf{0} & \mathbf{0} & \mathbb{\Lambda}_1(\mathbf{X})\mathbb{M}_1^{-1} & \mathbf{0} & \mathbf{0} & \mathbf{0} & \mathbf{0} \\ \mathbf{0} & \mathbf{0} & \frac{1}{\mathfrak{h}}\mathbb{S} & \mathbf{0} & \mathbf{0} & \mathbf{0} & \mathbf{0} & \mathbf{0} \\ \mathbf{0} & -\mathbb{M}_1^{-1}\mathbb{\Lambda}_1(\mathbf{X})^\top & \mathbf{0} & \mathbf{0} & \mathbf{0} & \mathbf{0} & \mathbf{0} & \mathbf{0} \\ \mathbf{0} & \mathbf{0} & \mathbf{0} & \mathbf{0} & \mathbf{0} & \mathbf{0} & \mathbb{M}_0^{-1} & \mathbf{0} \\ \mathbf{0} & \mathbf{0} & \mathbf{0} & \mathbf{0} & \mathbf{0} & \mathbf{0} & \mathbf{0} & \mathbb{M}_0^{-1} \\ \mathbf{0} & \mathbf{0} & \mathbf{0} & \mathbf{0} & -\mathbb{M}_0^{-1} & \mathbf{0} & \mathbf{0} & \mathbf{0} \\ \mathbf{0} & \mathbf{0} & \mathbf{0} & \mathbf{0} & \mathbf{0} & -\mathbb{M}_0^{-1} & \mathbf{0} & \mathbf{0} \end{pmatrix}. \tag{14}$$

With the notations (12), Hamiltonian (2) is discretized as

$$\begin{aligned} H(\mathbf{u}) = &\sum_{a=1}^{N_p} \omega_a (\sqrt{1 + p_a^2 + |\mathbf{A}_{\perp,h}(x_a)|^2} - 1) - \mathfrak{h}\, \mathbf{a}_3^\top \mathbb{G}^\top \mathbb{\Lambda}_1(\mathbf{X})^\top \mathbb{W} \mathbf{S}_2 + \mathfrak{h}\, \mathbf{a}_2^\top \mathbb{G}^\top \mathbb{\Lambda}_1(\mathbf{X})^\top \mathbb{W} \mathbf{S}_3, \\ &+ \frac{1}{2}\mathbf{e}_1^\top \mathbb{M}_1 \mathbf{e}_1 + \frac{1}{2}\mathbf{e}_2^\top \mathbb{M}_0 \mathbf{e}_2 + \frac{1}{2}\mathbf{e}_3^\top \mathbb{M}_0 \mathbf{e}_3 + \frac{1}{2}\mathbf{a}_2^\top \mathbb{G}^\top \mathbb{M}_1 \mathbb{G} \mathbf{a}_2 + \frac{1}{2}\mathbf{a}_3^\top \mathbb{G}^\top \mathbb{M}_1 \mathbb{G} \mathbf{a}_3, \end{aligned} \tag{15}$$

where the first term is the kinetic energy of particles. From the discrete Poisson bracket (13)-(14) and the discrete Hamiltonian (15), the equations after semi-discretization read as

$$\dot{\mathbf{u}} = \{\mathbf{u}, H\} = \mathbb{J}(\mathbf{u}) \nabla_{\mathbf{u}} H, \quad \mathbf{u}(t=0) = \mathbf{u}_0, \tag{16}$$

where $\dot{\mathbf{u}}(t) = \frac{\mathrm{d}}{\mathrm{d}t}\mathbf{u}(t)$.

3.2 Two dimensional case

In the two dimensional case, we regard A_3, E_3 as 0-forms, $\mathbf{E}_{12}$ as a 1-form, B_3 as a 2-form. The finite element spaces V_0, V_1, V_2 and projectors Π_0, Π_1, Π_2 are chosen to make the following diagram commute [32],

$$\begin{array}{ccccc} H^1 & \xrightarrow{\nabla} & H(\mathrm{curl}) & \xrightarrow{\nabla\times} & L^2 \\ \downarrow{\scriptstyle \Pi_0} & & \downarrow{\scriptstyle \Pi_1} & & \downarrow{\scriptstyle \Pi_2} \\ V_0 & \xrightarrow{\nabla} & V_1 & \xrightarrow{\nabla\times} & V_2 \end{array}$$

In the following, we describe the discretization of the two dimensional case with periodic boundary condition. We assume a set of uniform grids on spatial domain $[0, L_1] \times [0, L_2]$ with $\Delta x_i = L_i / M_i, i = 1, 2$. Similar to one dimensional case, we introduce the B-splines and D-splines in each direction,

$$N_i^{q_j}(x_j),\ 0 \le i \le n_N^i - 1, \quad D_i^{q_j - 1}(x_j),\ 0 \le i \le n_D^i - 1, \quad j = 1, 2. \tag{17}$$

By the tensor products of B-splines, we have the following sets of functions, which are used to build basis functions of finite element spaces.

$$
\begin{aligned}
&\left\{\Lambda_i^0(\mathbf{x}) = N_{i_1}^{p_1}(x_1)N_{i_2}^{p_2}(x_2), \quad N^0 = n_N^1 n_N^2, \quad i = n_N^2 i_1 + i_2.\right.\\
&\begin{cases}\Lambda_{1,i}^1(\mathbf{x}) := D_{i_1}^{p_1-1}(x_1)N_{i_2}^{p_2}(x_2), & N_1^1 = n_D^1 n_N^2, \quad i = n_N^2 i_1 + i_2,\\ \Lambda_{2,i}^1(\mathbf{x}) := N_{i_1}^{p_1}(x_1)D_{i_2}^{p_2-1}(x_2), & N_2^1 = n_N^1 n_D^2, \quad i = n_D^2 i_1 + i_2.\end{cases}\\
&\left\{\Lambda_i^2(\mathbf{x}) = N_{i_1}^{p_1-1}(x_1)N_{i_2}^{p_2-1}(x_2), \quad N^2 = n_D^1 n_D^2, \quad i = n_D^2 i_1 + i_2.\right.
\end{aligned}
$$

Then we have the following four finite element spaces and approximations of field unknowns [43, 23]

$$
\begin{aligned}
V_0 &:= \operatorname{span}\{\Lambda_i^0 | 0 \le i < N^0\}, && \ni \begin{cases} A_{3,h} = \sum_{i=0}^{N^0-1} a_{3,i}\Lambda_i^0 = (\mathbf{\Lambda}^0)^\top \mathbf{a}_3, \\ E_{3,h} = \sum_{i=0}^{N^0-1} e_{3,i}\Lambda_i^0 = (\mathbf{\Lambda}^0)^\top \mathbf{e}_3, \end{cases}\\
V_1 &:= \operatorname{span}\left\{ \begin{pmatrix} \Lambda_{1,i}^1 \\ 0 \end{pmatrix}, \begin{pmatrix} 0 \\ \Lambda_{2,i}^1 \end{pmatrix} \middle| \begin{matrix} 0 \le i < N_1^1 \\ 0 \le i < N_2^1 \end{matrix} \right\} && \ni \mathbf{E}_{12,h} = \sum_{j=1}^{2} \sum_{i=0}^{N_j^1-1} e_{12,j,i}\Lambda_{j,i}^1 \hat{\mathbf{e}}_j = (\mathbf{\Lambda}^1)^\top \mathbf{e}_{12},\\
V_1^* &:= \operatorname{span}\left\{ \begin{pmatrix} \Lambda_{2,i}^1 \\ 0 \end{pmatrix}, \begin{pmatrix} 0 \\ \Lambda_{1,i}^1 \end{pmatrix} \middle| \begin{matrix} 0 \le i < N_2^1 \\ 0 \le i < N_1^1 \end{matrix} \right\} && \ni \mathbf{B}_{12,h} = \sum_{j=1}^{2} \sum_{i=0}^{N_{3-\mu}^1-1} b_{12,j,i}\Lambda_{3-j,i}^1 \hat{\mathbf{e}}_j = (\mathbf{\Lambda}^*)^\top \mathbf{b}_{12},\\
V_2 &:= \operatorname{span}\{\Lambda_i^2 | 0 \le i < N^2\}, && \ni \mathbf{B}_{3,h} = \sum_{i=0}^{N^2-1} b_{3,i}\Lambda_i^2 = (\mathbf{\Lambda}^2)^\top \mathbf{b}_3,
\end{aligned}
\tag{18}
$$

where $\hat{\mathbf{e}}_j$ is the unit vector in x_j direction, $j \in \{1, 2\}$. The matrices of linear operators ∇, $\nabla\times$, and $\nabla^\top$ are denoted as $\mathbb{G}$, $\mathbb{C}$, and $\mathbb{G}_*$ with sizes $N^1 \times N^0$, $N^2 \times N^1$, $N^1 \times N^0$, respectively, where $N^1 = N_1^1 + N_2^1$. Next we introduce some notations used for the presentations of discrete Poisson

bracket and Hamiltonian with a slight abuse of notations with (12).

$$
\begin{aligned}
&\mathbf{X} := (x_{0,1}, \cdots, x_{N_p-1,1}, x_{0,2}, \cdots, x_{N_p-1,2})^\top \in \mathbb{R}^{2N_p},\\
&\mathbf{P} := (p_{0,1}, \cdots, p_{N_p-1,1}, p_{0,2}, \cdots, p_{N_p-1,2})^\top \in \mathbb{R}^{2N_p},\\
&\mathbf{S}_i := (s_{0,i}, \cdots, s_{N_p-1,i})^\top \ (i \in \{1,2,3\}) \ \in \mathbb{R}^{N_p}, \quad \mathbf{S}_{12} := (\mathbf{S}_1^\top, \mathbf{S}_2^\top)^\top \in \mathbb{R}^{2N_p},\\
&\mathbf{S} := (s_{0,1}, s_{0,2}, s_{0,3}, \cdots, s_{N_p-1,1}, s_{N_p-1,2}, s_{N_p-1,3})^\top \in \mathbb{R}^{3N_p},\\
&\mathbb{\Lambda}_0(\mathbf{X}) := (\Lambda_i^0(\mathbf{x}_a))_{0\le a<N_p, 0\le i<n_N} \in \mathbb{R}^{N_p\times N^0}, \quad \mathbb{\Lambda}_2(\mathbf{X}) := (\Lambda_i^2(\mathbf{x}_a))_{0\le a<N_p, 0\le i<n_D} \in \mathbb{R}^{N_p\times N^2},\\
&\mathbb{P}_\mu(\mathbf{H}) := (\Lambda^1_{\mu,i}(\mathbf{x}_a))_{0\le a<N_p, 0\le i<N^1_\mu} \quad (\mu \in \{1,2\}) \in \mathbb{R}^{N_p\times N^1_\mu},\\
&\mathbb{\Lambda}_1(\mathbf{X}) := \mathrm{diag}(\mathbb{P}_1, \mathbb{P}_2) \in \mathbb{R}^{2N_p\times N^1}, \quad \mathbb{\Lambda}_*(\mathbf{X}) := \mathrm{diag}(\mathbb{P}_2, \mathbb{P}_1) \in \mathbb{R}^{2N_p\times N^n},\\
&\mathbb{W} := \mathrm{diag}(\omega_0, \cdots, \omega_{N_p-1}) \in \mathbb{R}^{N_p\times N_p},\\
&\mathbb{S} = \mathrm{diag}(\mathbb{S}_0, \cdots, \mathbb{S}_{N_p-1}) \in \mathbb{R}^{3N_p\times 3N_p}, \quad \mathbb{S}_a = \frac{1}{\omega_a}\begin{pmatrix} 0 & s_{a,3} & -s_{a,2}\\ -s_{a,3} & 0 & s_{a,1}\\ s_{a,2} & -s_{a,1} & 0\end{pmatrix}, \ 0\le a<N_p,\\
&\mathbb{S}^p = \mathrm{diag}(\mathbb{S}^p_1, \cdots, \mathbb{S}^p_{N_p}) \in \mathbb{R}^{2N_p\times 2N_p}, \quad \mathbb{S}^p_a = \frac{1}{\omega_a}\begin{pmatrix} 0 & B_{3,h}(\mathbf{x}_a)\\ -B_{3,h}(\mathbf{x}_a) & 0\end{pmatrix}, \ 0\le a<N_p,\\
&\mathbb{M}_0 := \int_0^L \mathbf{\Lambda}^0(x)(\mathbf{\Lambda}^0(x))^\top \mathrm{d}x \in \mathbb{R}^{N^0\times N^0}, \quad \mathbb{M}_1 := \int_0^L \mathbf{\Lambda}^1(x)\cdot(\mathbf{\Lambda}^1(x))^\top \mathrm{d}x \in \mathbb{R}^{N^1\times N^1},\\
&\mathbb{M}_2 := \int_0^L \mathbf{\Lambda}^2(x)(\mathbf{\Lambda}^2(x))^\top \mathrm{d}x \in \mathbb{R}^{N^2\times N^2}, \quad \mathbb{M}_* := \int_0^L \mathbf{\Lambda}^*(x)\cdot(\mathbf{\Lambda}^*(x))^\top \mathrm{d}x \in \mathbb{R}^{N^1\times N^1}.
\end{aligned}
\tag{19}
$$

$\mathbb{M}_0, \mathbb{M}_1, \mathbb{M}_2, \mathbb{M}_*$ are called mass matrices of V_0, V_1, V_2, V_1^*, respectively. Distribution function is discretized as the sum of N_p particles with constant weights as (11). By discretizing functional derivatives (see in appendix 7.1) in (7), we get the following discrete Poisson bracket

$$
\{F, G\} = (\nabla_{\mathbf{u}} F)^\top \mathbb{J}(\mathbf{u}) \nabla_{\mathbf{u}} G, \tag{20}
$$

where $\mathbf{u} = (\mathbf{X}^\top, \mathbf{P}^\top, \mathbf{S}^\top, \mathbf{e}_{12}^\top, \mathbf{b}_3^\top, \mathbf{e}_3^\top, \mathbf{a}_3^\top)^\top$ and the matrix $\mathbb{J}(\mathbf{u})$ is defined by

$$
\mathbb{J}(\mathbf{u}) = \begin{pmatrix}
\mathbf{0} & \mathbb{W}^{-1} & \mathbf{0} & \mathbf{0} & \mathbf{0} & \mathbf{0} & \mathbf{0}\\
-\mathbb{W}^{-1} & \mathbb{S}^p & \mathbf{0} & \mathbb{\Lambda}_1(\mathbf{X})\mathbb{M}_1^{-1} & \mathbf{0} & \mathbf{0} & \mathbf{0}\\
\mathbf{0} & \mathbf{0} & \frac{1}{\mathfrak{h}}\mathbb{S} & \mathbf{0} & \mathbf{0} & \mathbf{0} & \mathbf{0}\\
\mathbf{0} & -\mathbb{M}_1^{-1}\mathbb{\Lambda}_1(\mathbf{X})^\top & \mathbf{0} & \mathbf{0} & \mathbb{M}_1^{-1}\mathbb{C}^\top & \mathbf{0} & \mathbf{0}\\
\mathbf{0} & \mathbf{0} & \mathbf{0} & -\mathbb{C}\mathbb{M}_1^{-1} & \mathbf{0} & \mathbf{0} & \mathbf{0}\\
\mathbf{0} & \mathbf{0} & \mathbf{0} & \mathbf{0} & \mathbf{0} & \mathbf{0} & \mathbb{M}_0^{-1}\\
\mathbf{0} & \mathbf{0} & \mathbf{0} & \mathbf{0} & \mathbf{0} & -\mathbb{M}_0^{-1} & \mathbf{0}
\end{pmatrix}. \tag{21}
$$

Hamiltonian (8) is discretized as

$$
\begin{aligned}
H(\mathbf{u}) = &\sum_{a=1}^{N_p} \omega_a(\sqrt{1+|\mathbf{p}_a|^2+|A_{3,h}(\mathbf{x}_a)|^2}-1) + \frac{1}{2}\mathbf{b}_3^\top\mathbb{M}_2\mathbf{b}_3 + \frac{1}{2}\mathbf{e}_{12}^\top\mathbb{M}_1\mathbf{e}_{12} + \frac{1}{2}\mathbf{e}_3^\top\mathbb{M}_0\mathbf{e}_3\\
&+ \frac{1}{2}\mathbf{a}_3^\top\mathbb{G}_*^\top\mathbb{M}_*\mathbb{G}_*\mathbf{a}_3 + \mathfrak{h}\,\mathbf{a}_3^\top\mathbb{G}_*^\top\mathbb{\Lambda}_*(\mathbf{X})^\top\mathbb{W}\mathbf{S}_{12} + \mathfrak{h}\,\mathbf{b}_3^\top\mathbb{\Lambda}_2(\mathbf{X})^\top\mathbb{W}\mathbf{S}_3,
\end{aligned}
\tag{22}
$$

where the first term is the kinetic energy of particles. With (20) and (22), we obtain a time-continuous finite dimensional Hamiltonian system

$$\dot{\mathbf{u}} = \{\mathbf{u}, H\} = \mathbb{J}(\mathbf{u})\nabla_{\mathbf{u}} H, \quad \mathbf{u}(t=0) = \mathbf{u}_0. \tag{23}$$

4 Time discretization

In this section, we introduce the time discretizations for (16) and (23). For general Hamiltonian systems, there is a method called Hamiltonian splitting, which can preserve the geometric structures and show very good long time behaviors [17]. This method requires all the Hamiltonian subsystems explicitly solvable, such as [23]. However, this is not true for our Hamiltonian systems (16) and (23). The difficulty comes from the kinetic energy parts in Hamiltonians (15) and (22), which give non-solvable subsystems.

Alternatively, we use Poisson splittings (to split the Poisson matrix and obtain several subsystems as [27]) combined with discrete gradient methods to our time continuous finite dimensional Hamiltonian systems. The proposed schemes are energy-conserving and the numerical solutions satisfy the discrete Poisson equations. In the following sections, Δt is the uniform time step size, approximate solutions of unknowns $\mathbf{u}$ at $n\Delta t$ are denoted by $\mathbf{u}^n$ and $\mathbf{u}^{n+\frac{1}{2}} = \frac{\mathbf{u}^n + \mathbf{u}^{n+1}}{2}$.

Discrete gradient method For the following conservative ordinary equations with an invariant $H(\mathbf{u})$,

$$\dot{\mathbf{u}} = \mathbb{J}(\mathbf{u})\nabla H(\mathbf{u}), \quad \mathbb{J}(\mathbf{u})^\top = -\mathbb{J}(\mathbf{u}), \quad \mathbf{u} \in \mathbb{R}^n, \tag{24}$$

$\bar{\nabla} H(\mathbf{u}^n, \mathbf{u}^{n+1})$ is called a discrete gradient [44] for time step $[t_n, t_{n+1}]$, if

$$(\mathbf{u}^{n+1} - \mathbf{u}^n)^\top \bar{\nabla} H(\mathbf{u}^n, \mathbf{u}^{n+1}) = H(\mathbf{u}^{n+1}) - H(\mathbf{u}^n).$$

With the help of the discrete gradient, we obtain the following energy conserving scheme,

$$\frac{\mathbf{u}^{n+1} - \mathbf{u}^n}{\Delta t} = \bar{\mathbb{J}}(\mathbf{u}^n, \mathbf{u}^{n+1})\bar{\nabla} H(\mathbf{u}^n, \mathbf{u}^{n+1}),$$

where $\bar{\mathbb{J}}(\mathbf{u}^n, \mathbf{u}^{n+1})$ is any anti-symmetric approximation of $\mathbb{J}(\mathbf{u})$, such as midpoint approximation $\mathbb{J}(\frac{\mathbf{u}^n + \mathbf{u}^{n+1}}{2})$. In subsections 4.1 and 4.2, first order discrete gradient proposed in [36] is applied for the above one and two dimensional models (16) (23), respectively. In subsection 4.3, second order midpoint discrete gradient proposed in [14] is also considered.

4.1 One dimensional case

For (16), we firstly split the matrix (14) into following three parts,

$$\mathbb{J}_1(\mathbf{u}) = \begin{pmatrix} & & \mathbf{0} & & \\ & \mathbf{0} & \mathbf{0} & \mathbb{M}_0^{-1} & \mathbf{0} \\ \mathbf{0} & \mathbf{0} & \mathbf{0} & \mathbf{0} & \mathbb{M}_0^{-1} \\ & -\mathbb{M}_0^{-1} & \mathbf{0} & \mathbf{0} & \mathbf{0} \\ & \mathbf{0} & -\mathbb{M}_0^{-1} & \mathbf{0} & \mathbf{0} \end{pmatrix}, \quad \mathbb{J}_2(\mathbf{u}) = \begin{pmatrix} \mathbf{0} & \mathbf{0} & \mathbf{0} & & \\ \mathbf{0} & \mathbf{0} & \mathbf{0} & \mathbf{0} & \\ \mathbf{0} & \mathbf{0} & \frac{1}{\mathfrak{h}}\mathbb{S} & & \\ & & \mathbf{0} & & \end{pmatrix},$$

$$\mathbb{J}_3(\mathbf{u}) = \begin{pmatrix} \mathbf{0} & \mathbb{W}^{-1} & \mathbf{0} & \mathbf{0} & \\ -\mathbb{W}^{-1} & \mathbf{0} & \mathbf{0} & \mathbb{A}_1(\mathbf{X})\mathbb{M}_1^{-1} & \mathbf{0} \\ \mathbf{0} & \mathbf{0} & \mathbf{0} & \mathbf{0} & \\ \mathbf{0} & -\mathbb{M}_1^{-1}\mathbb{A}_1(\mathbf{X})^\top & \mathbf{0} & \mathbf{0} & \\ & & \mathbf{0} & & \end{pmatrix}.$$

Then we have three corresponding subsystems,

$$\dot{\mathbf{u}} = \mathbb{J}_1(\mathbf{u})\nabla_{\mathbf{u}}H, \quad ,\dot{\mathbf{u}} = \mathbb{J}_2(\mathbf{u})\nabla_{\mathbf{u}}H, \quad \dot{\mathbf{u}} = \mathbb{J}_3(\mathbf{u})\nabla_{\mathbf{u}}H.$$

Subsystem I The first subsystem $\dot{\mathbf{u}} = \mathbb{J}_1(\mathbf{u})\nabla_{\mathbf{u}}H$ about $(\mathbf{e}_2, \mathbf{e}_3, \mathbf{a}_2, \mathbf{a}_3)$ is

$$\begin{aligned}
\dot{\mathbf{e}}_2 &= \mathbb{M}_0^{-1}\left(\sum_{a=1}^{N_p}\frac{\omega_a}{\sqrt{1+p_a^2+|\mathbf{A}_\perp(x_a)|^2}}\mathbf{\Lambda}^0(x_a)A_{2,h} + \mathbb{G}^\top\mathbb{M}_1\mathbb{G}\mathbf{a}_2\right) + \mathfrak{h}\,\mathbb{M}_0^{-1}\mathbb{G}^\top\mathbb{\Lambda}_1(\mathbf{X})^\top\mathbb{W}\mathbf{S}_3,\\
\dot{\mathbf{e}}_3 &= \mathbb{M}_0^{-1}\left(\sum_{a=1}^{N_p}\frac{\omega_a}{\sqrt{1+p_a^2+|\mathbf{A}_\perp(x_a)|^2}}\mathbf{\Lambda}^0(x_a)A_{3,h} + \mathbb{G}^\top\mathbb{M}_1\mathbb{G}\mathbf{a}_3\right) - \mathfrak{h}\,\mathbb{M}_0^{-1}\mathbb{G}^\top\mathbb{\Lambda}_1(\mathbf{X})^\top\mathbb{W}\mathbf{S}_2,\\
\dot{\mathbf{a}}_2 &= -\mathbf{e}_2,\ \dot{\mathbf{a}}_3 = -\mathbf{e}_3.
\end{aligned}$$

With the discrete gradients introduced in [36], we have

$$\begin{aligned}
&\bar{\nabla}_{\mathbf{e}_2}H = \mathbb{M}_0\mathbf{e}_2^{n+\frac{1}{2}}, \quad \bar{\nabla}_{\mathbf{e}_3}H = \mathbb{M}_0\mathbf{e}_3^{n+\frac{1}{2}},\\
&\bar{\nabla}_{\mathbf{a}_2}H = \sum_a w_a\frac{(A_{2,h}^{n+1}(x_a^n)+A_{2,h}^n(x_a^n))\mathbf{\Lambda}^0(x_a^n)}{\gamma(p_a^n,\mathbf{A}_{\perp,h}^{n+1}(x_a^n))+\gamma(p_a^n,\mathbf{A}_{\perp,h}^n(x_a^n))} + \mathbb{G}^\top\mathbb{M}_1\mathbb{G}\mathbf{a}_2^{n+\frac{1}{2}} + \mathfrak{h}\,\mathbb{G}^\top\mathbb{\Lambda}_1(\mathbf{X}^n)^\top\mathbb{W}\mathbf{S}_3^n,\\
&\bar{\nabla}_{\mathbf{a}_3}H = \sum_a w_a\frac{(A_{3,h}^{n+1}(x_a^n)+A_{3,h}^n(x_a^n))\mathbf{\Lambda}^0(x_a^n)}{\gamma(p_a^n,\mathbf{A}_{\perp,h}^{n+1}(x_a^n))+\gamma(p_a^n,\mathbf{A}_{\perp,h}^n(x_a^n))} + \mathbb{G}^\top\mathbb{M}_1\mathbb{G}\mathbf{a}_3^{n+\frac{1}{2}} - \mathfrak{h}\,\mathbb{G}^\top\mathbb{\Lambda}_1(\mathbf{X}^n)^\top\mathbb{W}\mathbf{S}_2^n,
\end{aligned}$$

and the following scheme,

$$\begin{aligned}
&\frac{\mathbf{e}_2^{n+1}-\mathbf{e}_2^n}{\Delta t} = \mathbb{M}_0^{-1}\bar{\nabla}_{\mathbf{a}_2}H, \quad \frac{\mathbf{e}_3^{n+1}-\mathbf{e}_3^n}{\Delta t} = \mathbb{M}_0^{-1}\bar{\nabla}_{\mathbf{a}_3}H,\\
&\frac{\mathbf{a}_2^{n+1}-\mathbf{a}_2^n}{\Delta t} = -\mathbb{M}_0^{-1}\bar{\nabla}_{\mathbf{e}_2}H, \quad \frac{\mathbf{a}_3^{n+1}-\mathbf{a}_3^n}{\Delta t} = -\mathbb{M}_0^{-1}\bar{\nabla}_{\mathbf{e}_3}H.
\end{aligned}$$

Substituting the above last two equations into the first two equations gives

$$\begin{aligned}
\left(\mathbb{M}_0+\frac{\Delta t^2}{4}\mathbb{G}^\top\mathbb{M}_1\mathbb{G}\right)\mathbf{e}_2^{n+1} &= \left(\mathbb{M}_0-\frac{\Delta t^2}{4}\mathbb{G}^\top\mathbb{M}_1\mathbb{G}\right)\mathbf{e}_2^n + \Delta t\mathbb{G}^\top\mathbb{M}_1\mathbb{G}\mathbf{a}_2^n + \Delta t\mathfrak{h}\,\mathbb{G}^\top\mathbb{\Lambda}_1(\mathbf{X}^n)^\top\mathbb{W}\mathbf{S}_3\\
&\quad + \Delta t\sum_{a=1}^{N_p}\frac{\omega_a(A_{2,h}^{n+1}(x_a^n)+A_{2,h}^n(x_a^n))\mathbf{\Lambda}^0(x_a^n)}{\gamma(p_a^n,\mathbf{A}_{\perp,h}^{n+1}(x_a^n))+\gamma(p_a^n,\mathbf{A}_{\perp,h}^n(x_a^n))},\\
\left(\mathbb{M}_0+\frac{\Delta t^2}{4}\mathbb{G}^\top\mathbb{M}_1\mathbb{G}\right)\mathbf{e}_3^{n+1} &= \left(\mathbb{M}_0-\frac{\Delta t^2}{4}\mathbb{G}^\top\mathbb{M}_1\mathbb{G}\right)\mathbf{e}_3^n + \Delta t\mathbb{G}^\top\mathbb{M}_1\mathbb{G}\mathbf{a}_3^n - \Delta t\mathfrak{h}\,\mathbb{G}^\top\mathbb{\Lambda}_1(\mathbf{X}^n)^\top\mathbb{W}\mathbf{S}_2\\
&\quad + \Delta t\sum_{a=1}^{N_p}\frac{\omega_a(A_{3,h}^{n+1}(x_a^n)+A_{3,h}^n(x_a^n))\mathbf{\Lambda}^0(x_a^n)}{\gamma(p_a^n,\mathbf{A}_{\perp,h}^{n+1}(x_a^n))+\gamma(p_a^n,\mathbf{A}_{\perp,h}^n(x_a^n))},
\end{aligned} \tag{25}$$

where on the right side $A_{2,h}^{n+1}, A_{3,h}^{n+1}$ are represented with $\mathbf{e}_2^n, \mathbf{e}_2^{n+1}, \mathbf{e}_3^n, \mathbf{e}_3^{n+1}$ using the equation $\frac{\mathbf{a}_2^{n+1}-\mathbf{a}_2^n}{\Delta t} = -\frac{\mathbf{e}_2^n+\mathbf{e}_2^{n+1}}{2}$, $\frac{\mathbf{a}_3^{n+1}-\mathbf{a}_3^n}{\Delta t} = -\frac{\mathbf{e}_3^n+\mathbf{e}_3^{n+1}}{2}$. To solve the above scheme about $\mathbf{e}_2^{n+1}, \mathbf{e}_3^{n+1}$, a fixed point iteration method is used with a pre-conditioner $\mathbb{M}_0^{-1}$ computed by fast Fourier transformation as $\mathbb{M}_0$ is circulant. During each iteration, a loop of all the particles is required to compute the terms containing $\mathbf{A}_{\perp,h}^{n+1}(x_a^n), 0 \le a < N_p$ on the right hand side of (25). The solution map from n-th to $(n+1)$-th time step is denoted as $\Phi_{e23a23}^n(\Delta t)$.

Subsystem II The second subsystem $\dot{\mathbf{u}} = \mathbb{J}_2(\mathbf{u})\nabla_{\mathbf{u}}H$ about $\mathbf{S}$ is

$$\dot{\mathbf{S}} = \frac{1}{\mathfrak{h}}\mathbb{S}\nabla_{\mathbf{S}}H.$$

As Hamiltonian depends on $\mathbf{S}$ linearly, discrete gradient for $\mathbf{S}$ is just usual gradient, i.e., $\bar{\nabla}_{\mathbf{S}}H = \nabla_{\mathbf{S}}H$. For the a-th particle, we have

$$\dot{\mathbf{s}}_a = \begin{pmatrix} \dot{s}_{a,1} \\ \dot{s}_{a,2} \\ \dot{s}_{a,3} \end{pmatrix} = \begin{pmatrix} 0 & Y_a & Z_a \\ -Y_a & 0 & 0 \\ -Z_a & 0 & 0 \end{pmatrix} \begin{pmatrix} s_{a,1} \\ s_{a,2} \\ s_{a,3} \end{pmatrix} =: \hat{r}_a \mathbf{s}_a, \tag{26}$$

where $Y_a = (\mathbf{a}_2^{n+1})^\top \mathbb{G}^\top \mathbf{\Lambda}^1(x_a^n)$, $Z_a = (\mathbf{a}_3^{n+1})^\top \mathbb{G}^\top \mathbf{\Lambda}^1(x_a^n)$. The Rodrigues' formula gives the following explicit solution for (26)

$$\mathbf{s}_a^{n+1} = \exp(\Delta t \hat{r}_a)\mathbf{s}_a(t^n) = \left(I + \frac{\sin(\Delta t|\mathbf{r}_a|)}{|\mathbf{r}_a|}\hat{r}_a + \frac{1}{2}\left(\frac{\sin(\frac{\Delta t}{2}|\mathbf{r}_a|)}{\frac{|\mathbf{r}_a|}{2}} \right)^2 \hat{r}_a^2 \right) \mathbf{s}_a^n, \tag{27}$$

where $\mathbf{r}_a = (0, Z_a, -Y_a)^\top \in \mathbb{R}^3$, and I is the 3×3 identity matrix. The solution map from n-th to $(n+1)$-th time step is denoted as $\Phi_s^n(\Delta t)$.

Subsystem III The third subsystem $\dot{\mathbf{u}} = \mathbb{J}_3(\mathbf{u})\nabla_{\mathbf{u}}H$ about variables $x_a, p_a, \mathbf{e}_1, 0 \le a < N_p$ is

$$\begin{aligned}
\dot{x}_a &= \frac{p_a}{\gamma(p_a, \mathbf{A}_{\perp,h}(x_a))}, \\
\dot{p}_a &= E_{1,h}(x_a) - \frac{\mathbf{A}_{\perp,h}(x_a) \cdot \partial_x \mathbf{A}_{\perp,h}(x_a)}{\gamma(p_a, \mathbf{A}_{\perp,h}(x_a))} - \mathfrak{h} s_2^a \partial_x^2 A_{3,h}(x_a) + \mathfrak{h} s_3^a \partial_x^2 A_{2,h}(x_a),\ 0 \le a < N_p, \\
\dot{\mathbf{e}}_1 &= -\mathbb{M}_1^{-1} \sum_{a=1}^{N_p} \frac{w_a p_a \mathbf{\Lambda}^1(x_a)}{\gamma(p_a, \mathbf{A}_{\perp,h}(x_a))}.
\end{aligned}$$

With the following discrete gradients,

$$\begin{aligned}
\bar{\nabla}_{x_a}H &= w_a \frac{\left(\mathbf{A}_{\perp,h}^n(x_a^{n+1}) + \mathbf{A}_{\perp,h}^n(x_a^n) \right) \cdot \frac{\left(\mathbf{A}_{\perp,h}^n(x_a^{n+1}) - \mathbf{A}_{\perp,h}^n(x_a^n) \right)}{(x_a^{n+1} - x_a^n)}}{\gamma(p_a^n, \mathbf{A}_{\perp,h}^n(x_a^{n+1})) + \gamma(p_a^n, \mathbf{A}_{\perp,h}^n(x_a^n))} \\
&+ w_a \mathfrak{h} s_{a,y}^{n+1} \left(\frac{\partial_x A_{z,h}^{n+1}(x_a^{n+1}) - \partial_x A_{z,h}^{n+1}(x_a^n)}{x_a^{n+1} - x_a^n} \right) - w_a \mathfrak{h} s_{a,z}^{n+1} \left(\frac{\partial_x A_{y,h}^{n+1}(x_a^{n+1}) - \partial_x A_{y,h}^{n+1}(x_a^n)}{x_a^{n+1} - x_a^n} \right), \\
\bar{\nabla}_{p_a}H &= w_a \frac{p_a^n + p_a^{n+1}}{\gamma(p_a^n, \mathbf{A}_{\perp,h}^{n+1}(x_a^{n+1})) + \gamma(p_a^{n+1}, \mathbf{A}_{\perp,h}^{n+1}(x_a^{n+1}))}, \\
\bar{\nabla}_{\mathbf{e}_1}H &= \mathbb{M}_1 \mathbf{e}_1^{n+\frac{1}{2}},
\end{aligned}$$

the scheme for this subsystem reads

$$\frac{\dot{x_a^{n+1}} - x_a^n}{\Delta t} = \frac{p_a^n + p_a^{n+1}}{\gamma(p_a^n, \mathbf{A}_{\perp,h}^{n+1}(x_a^{n+1})) + \gamma(p_a^{n+1}, \mathbf{A}_{\perp,h}^{n+1}(x_a^{n+1}))},$$

$$\frac{p_a^{n+1} - p_a^n}{\Delta t} = \frac{1}{\Delta t}\int_{t^n}^{t^{n+1}} \mathbb{\Lambda}_1(\mathbf{X}(\tau))\mathrm{d}\tau \mathbf{e}_1^{n+\frac{1}{2}} - \frac{\left(\mathbf{A}_{\perp,h}^{n+1}(x_a^{n+1}) + \mathbf{A}_{\perp,h}^{n+1}(x_a^n)\right)\cdot \frac{\mathbf{A}_{\perp,h}^{n+1}(x_a^{n+1}) - \mathbf{A}_{\perp,h}^{n+1}(x_a^n)}{x_a^{n+1}-x_a^n}}{\gamma(p_a^n, \mathbf{A}_{\perp,h}^{n+1}(x_a^{n+1})) + \gamma(p_a^n, \mathbf{A}_{\perp,h}^{n+1}(x_a^n))}$$

$$- \mathfrak{h} s_{a,y}^{n+1}\left(\frac{\partial_x A_{3,h}^{n+1}(x_a^{n+1}) - \partial_x A_{3,h}^{n+1}(x_a^n)}{x_a^{n+1} - x_a^n}\right) + \mathfrak{h} s_{a,z}^{n+1}\left(\frac{\partial_x A_{2,h}^{n+1}(x_a^{n+1}) - \partial_x A_{2,h}^{n+1}(x_a^n)}{x_a^{n+1} - x_a^n}\right),$$

$$\frac{\mathbf{e}_1^{n+1} - \mathbf{e}_1^n}{\Delta t} = -\mathbb{M}_1^{-1}\sum_a \frac{1}{\Delta t}\int_{t^n}^{t^{n+1}} \mathbf{\Lambda}^1(x_a(\tau))^\top \mathrm{d}\tau w_a \frac{p_a^n + p_a^{n+1}}{\gamma(p_a^n, \mathbf{A}_{\perp,h}^{n+1}(x_a^{n+1})) + \gamma(p_a^{n+1}, \mathbf{A}_{\perp,h}^{n+1}(x_a^{n+1}))},$$

where the time-continuous trajectory is defined as

$$x_a(\tau) = x_a^n + (\tau - t^n)\frac{x_a^{n+1} - x_a^n}{\Delta t}, \quad \tau \in [t^n, t^{n+1}], \quad 0 \le a < N_p.$$

The solution map from n-th to $(n+1)$-th time step is denoted as $\Phi_{xpe1}^n(\Delta t)$.

Remark 1. *When x_a^n is very close to x_a^{n+1}, $\frac{\mathbf{A}_{\perp,h}^{n+1}(x_a^{n+1}) - \mathbf{A}_{\perp,h}^{n+1}(x_a^n)}{x_a^{n+1}-x_a^n}$ and $\frac{\partial_x \mathbf{A}_{\perp,h}^{n+1}(x_a^{n+1}) - \partial_x \mathbf{A}_{\perp,h}^{n+1}(x_a^n)}{x_a^{n+1}-x_a^n}$ are in the forms of $\frac{0}{0}$, which could be avoided by*

$$\frac{\mathbf{A}_{\perp,h}^{n+1}(x_a^{n+1}) - \mathbf{A}_{\perp,h}^{n+1}(x_a^n)}{x_a^{n+1} - x_a^n} \approx \partial_x \mathbf{A}_{\perp,h}^{n+1}\left(\frac{x_a^{n+1} + x_a^n}{2}\right), \frac{\partial_x \mathbf{A}_{\perp,h}^{n+1}(x_a^{n+1}) - \partial_x \mathbf{A}_{\perp,h}^{n+1}(x_a^n)}{x_a^{n+1} - x_a^n} \approx \partial_x^2 \mathbf{A}_{\perp,h}^{n+1}\left(\frac{x_a^{n+1} + x_a^n}{2}\right).$$

Remark 2. *The discrete Poisson equation $\mathbb{G}^\top \mathbb{M}_1 \mathbf{e}_1(t) = -\mathbb{\Lambda}_0(\mathbf{X})^\top \mathbb{W}\mathbb{1}_{N_p}$ is preserved. In fact, multiplying $\mathbb{G}^\top \mathbb{M}_1$ from left with the scheme about $\mathbf{e}_1$, we have*

$$\begin{aligned}
\mathbb{G}^\top \mathbb{M}_1 \mathbf{e}_1^{n+1} &= \mathbb{G}^\top \mathbb{M}_1 \mathbf{e}_1^n - \mathbb{G}^\top \sum_a \int_{t^n}^{t^{n+1}} \mathbf{\Lambda}^1(x_a(\tau))\mathrm{d}\tau w_a \frac{\mathrm{d}x_a(\tau)}{\mathrm{d}\tau}, \\
&= \mathbb{G}^\top \mathbb{M}_1 \mathbf{e}_1^n - \sum_a \int_{t^n}^{t^{n+1}} \frac{\mathrm{d}}{\mathrm{d}\tau}\mathbf{\Lambda}^0(x_a(\tau))w_a \mathrm{d}\tau, \\
&= \mathbb{G}^\top \mathbb{M}_1 \mathbf{e}_1^n - \mathbb{\Lambda}_0(\mathbf{X}^{n+1})^\top \mathbb{W}\mathbb{1}_{N_p} + \mathbb{\Lambda}_0(\mathbf{X}^n)^\top \mathbb{W}\mathbb{1}_{N_p},
\end{aligned}$$

where $\mathbb{1}_{N_p}$ is the vector of size N_p composed of 1. Then, the discrete Poisson equation (weak formulation) $\mathbb{G}^\top \mathbb{M}_1 \mathbf{e}_1(t) = -\mathbb{\Lambda}_0(\mathbf{X})^\top \mathbb{W}\mathbb{1}_{N_p}$ is always satisfied by the numerical solution if it holds initially.

Then using the following Lie splitting [17] gives us the first order approximate solution of (16),

$$\Phi(\mathbf{u}^n) = \Phi_{xpe1}^n(\Delta t)\Phi_s^n(\Delta t)\Phi_{e23a23}^n(\Delta t)\mathbf{u}^n. \tag{28}$$

4.2 Two dimensional case

For (23), we firstly split the matrix (21) into the following four parts,

$$\mathbb{J}_1(\mathbf{u}) = \begin{pmatrix} & & 0 & \\ & & \mathbf{0} & \mathbb{M}_0^{-1} \\ 0 & & -\mathbb{M}_0^{-1} & \mathbf{0} \end{pmatrix}, \quad \mathbb{J}_2(\mathbf{u}) = \begin{pmatrix} & 0 & & \\ & \mathbf{0} & \mathbb{M}_1^{-1}\mathbb{C}^\top & \mathbf{0} \quad \mathbf{0} \\ 0 & -\mathbb{C}\mathbb{M}_1^{-1} & \mathbf{0} & \mathbf{0} \quad \mathbf{0} \\ & \mathbf{0} & \mathbf{0} & \mathbf{0} \quad \mathbf{0} \\ & \mathbf{0} & \mathbf{0} & \mathbf{0} \quad \mathbf{0} \end{pmatrix},$$

$$\mathbb{J}_3(\mathbf{u}) = \begin{pmatrix} \mathbf{0} & \mathbf{0} & \mathbf{0} & \\ \mathbf{0} & \mathbb{S}^p & \mathbf{0} & 0 \\ \mathbf{0} & \mathbf{0} & \frac{1}{\mathfrak{h}}\mathbb{S} & \\ & & 0 & \end{pmatrix}, \quad \mathbb{J}_4(\mathbf{u}) = \begin{pmatrix} \mathbf{0} & \mathbb{W}^{-1} & \mathbf{0} & \mathbf{0} & \\ -\mathbb{W}^{-1} & \mathbf{0} & \mathbf{0} & \mathbb{A}_1(\mathbf{X})\mathbb{M}_1^{-1} & 0 \\ \mathbf{0} & \mathbf{0} & \mathbf{0} & \mathbf{0} & \\ \mathbf{0} & -\mathbb{M}_1^{-1}\mathbb{A}_1(\mathbf{X})^\top & \mathbf{0} & \mathbf{0} & \\ & & 0 & & \end{pmatrix}.$$

Then we have four corresponding subsystems,

$$\dot{\mathbf{u}} = \mathbb{J}_1(\mathbf{u})\nabla_{\mathbf{u}}H, \quad ,\dot{\mathbf{u}} = \mathbb{J}_2(\mathbf{u})\nabla_{\mathbf{u}}H, \quad \dot{\mathbf{u}} = \mathbb{J}_3(\mathbf{u})\nabla_{\mathbf{u}}H, \quad \dot{\mathbf{u}} = \mathbb{J}_4(\mathbf{u})\nabla_{\mathbf{u}}H.$$

Subsystem I The first subsystem $\dot{\mathbf{u}} = \mathbb{J}_1(\mathbf{u})\nabla_{\mathbf{u}}H$ is

$$\begin{aligned} &\dot{\mathbf{a}_3} = -\mathbf{e}_3, \\ &\dot{\mathbf{e}_3} = \mathbb{M}_0^{-1}\nabla_{\mathbf{a}_3}H = \mathbb{M}_0^{-1}\left(\mathbb{G}_*^\top\mathbb{M}_{1,*}\mathbb{G}_*\mathbf{a}_3 + \mathfrak{h}\mathbb{G}_*^\top\mathbb{A}_*(\mathbf{X})^\top\mathbb{W}\mathbf{S}_{12}\right) + \mathbb{M}_0^{-1}\sum_a w_a\frac{A_{3,h}(\mathbf{x}_a)\mathbf{\Lambda}^0(\mathbf{x}_a)}{\gamma(\mathbf{p}_a, A_3(\mathbf{x}_a))}. \end{aligned} \tag{29}$$

With the discrete gradients about $\mathbf{e}_3$ and $\mathbf{a}_3$,

$$\bar{\nabla}_{\mathbf{e}_3}H = \mathbb{M}_2\mathbf{e}_3^{n+\frac{1}{2}}, \ \bar{\nabla}_{\mathbf{a}_3}H = \mathbb{G}_*^\top\mathbb{M}_{1,*}\mathbb{G}_*\mathbf{a}_3^{n+\frac{1}{2}} + \mathfrak{h}\mathbb{G}_*^\top\mathbb{A}_*(\mathbf{X}^n)^\top\mathbb{W}\mathbf{S}_{12}^n + \sum_a w_a\frac{(A_{3,h}^n(\mathbf{x}_a^n) + A_{3,h}^{n+1}(\mathbf{x}_a^n))\mathbf{\Lambda}^0(\mathbf{x}_a)}{\gamma(\mathbf{p}_a^n, A_{3,h}^n(\mathbf{x}_a^n)) + \gamma(\mathbf{p}_a^n, A_{3,h}^{n+1}(\mathbf{x}_a^n))},$$

we have the following scheme,

$$\begin{aligned} &\frac{\mathbf{a}_3^{n+1} - \mathbf{a}_3^n}{\Delta t} = -\mathbf{e}_3^{n+\frac{1}{2}}, \\ &\frac{\mathbf{e}_3^{n+1} - \mathbf{e}_3^n}{\Delta t} = \mathbb{M}_0^{-1}\left(\mathbb{G}_*^\top\mathbb{M}_{1,*}\mathbb{G}_*\mathbf{a}_3^{n+\frac{1}{2}} + \mathfrak{h}\mathbb{G}_*^\top\mathbb{A}_*(\mathbf{X}^n)^\top\mathbb{W}\mathbf{S}_{12}^n\right) \\ &\qquad + \mathbb{M}_0^{-1}\sum_a w_a\frac{(A_{3,h}^n(\mathbf{x}_a^n) + A_{3,h}^{n+1}(\mathbf{x}_a^n))\mathbf{\Lambda}^0(\mathbf{x}_a^n)}{\gamma(\mathbf{p}_a^n, A_{3,h}^n(\mathbf{x}_a^n)) + \gamma(\mathbf{p}_a^n, A_{3,h}^{n+1}(\mathbf{x}_a^n))}. \end{aligned}$$

After substituting the above first equation into the second one, we get

$$\begin{aligned} \left(\mathbb{M}_0 + \frac{\Delta t^2}{4}\mathbb{G}_*^\top\mathbb{M}_*\mathbb{G}_*\right)\mathbf{e}_3^{n+1} = &\left(\mathbb{M}_0 - \frac{\Delta t^2}{4}\mathbb{G}_*^\top\mathbb{M}_*\mathbb{G}_*\right)\mathbf{e}_3^n + \Delta t\mathbb{G}_*^\top\mathbb{M}_*\mathbb{G}_*\mathbf{a}_3^n + \mathfrak{h}\Delta t\mathbb{G}_*^\top\mathbb{A}_*(\mathbf{X}^n)^\top\mathbb{W}\mathbf{S}_{xy} \\ &+ \Delta t\sum_a w_a\frac{(A_{3,h}^n(\mathbf{x}_a^n) + A_{3,h}^{n+1}(\mathbf{x}_a^n))\mathbf{\Lambda}^0(\mathbf{x}_a^n)}{\gamma(\mathbf{p}_a^n, A_{3,h}^n(\mathbf{x}_a^n)) + \gamma(\mathbf{p}_a^n, A_{3,h}^{n+1}(\mathbf{x}_a^n))}, \end{aligned} \tag{30}$$

where on the right side $A_{3,h}^{n+1}$ is represented with $\mathbf{e}_3^n, \mathbf{e}_3^{n+1}$ using the equation $\frac{\mathbf{a}_3^{n+1}-\mathbf{a}_3^n}{\Delta t} = -\frac{\mathbf{e}_3^n+\mathbf{e}_3^{n+1}}{2}$. Similarly, the fixed point iteration method is used to solve the above equation

about $\mathbf{e}_3^{n+1}$ with the inverse of $\mathbb{M}_0$ as a pre-conditioner. In each iteration, a loop of all the particles is required to compute the terms related with particles. The solution map from n-th to $(n+1)$-th time step is denoted as $\Phi^n_{e3a3}(\Delta t)$.

Subsystem II The second subsystem $\dot{\mathbf{u}} = \mathbb{J}_2(\mathbf{u})\nabla_{\mathbf{u}} H$ is

$$\begin{aligned}\dot{\mathbf{e}_{12}} &= \mathbb{M}_1^{-1}\mathbb{C}^\top \nabla_{\mathbf{b}_3} H = \mathbb{M}_1^{-1}\mathbb{C}^\top \left(\mathbb{M}_2\mathbf{b}_3 + \hbar\mathbb{A}_2(\mathbf{X})^\top \mathbb{W}\mathbf{S}_3\right),\\ \dot{\mathbf{b}_3} &= -\mathbb{C}\mathbb{M}_1^{-1}\nabla_{\mathbf{e}_{12}} H = -\mathbb{C}\mathbf{e}_{12}.\end{aligned} \tag{31}$$

With the discrete gradients about $\mathbf{e}_{12}$ and $\mathbf{b}_3$,

$$\bar{\nabla}_{\mathbf{e}_{12}} H = \mathbb{M}_1 \mathbf{e}_{12}^{n+\frac{1}{2}}, \quad \bar{\nabla}_{\mathbf{b}_3} H = \mathbb{M}_2 \mathbf{b}_3^{n+\frac{1}{2}} + \hbar\mathbb{A}_2(\mathbf{X}^n)^\top \mathbb{W}\mathbf{S}_3^n,$$

we have the following scheme,

$$\begin{aligned}\frac{\mathbf{e}_{12}^{n+1} - \mathbf{e}_{12}^n}{\Delta t} &= \mathbb{M}_1^{-1}\mathbb{C}^\top \left(\mathbb{M}_2\mathbf{b}_3^{n+\frac{1}{2}} + \hbar\mathbb{A}_2(\mathbf{X}^n)^\top \mathbb{W}\mathbf{S}_3^n\right),\\ \frac{\mathbf{b}_3^{n+1} - \mathbf{b}_3^n}{\Delta t} &= -\mathbb{C}\mathbf{e}_{12}^{n+\frac{1}{2}},\end{aligned} \tag{32}$$

from which we get

$$\left(\mathbb{M}_1 + \frac{\Delta t^2}{4}\mathbb{C}^\top\mathbb{M}_2\mathbb{C}\right)\mathbf{e}_{12}^{n+1} = \left(\mathbb{M}_1 - \frac{\Delta t^2}{4}\mathbb{C}^\top\mathbb{M}_2\mathbb{C}\right)\mathbf{e}_{12}^n + \Delta t\mathbb{C}^\top\mathbb{M}_2\mathbf{b}_3^n + \Delta t\hbar\mathbb{C}^\top\mathbb{A}_2(\mathbf{X}^n)^\top\mathbb{W}\mathbf{S}_3^n. \tag{33}$$

Again, as $\mathbb{M}_1$ is circulant, a fixed point iteration method is used to solve above equation with the inverse of $\mathbb{M}_1$ as a pre-conditioner by fast Fourier transformation. The solution map from n-th to $(n+1)$-th time step is denoted as $\Phi^n_{e12b3}(\Delta t)$.

Subsystem III The third subsystem $\dot{\mathbf{u}} = \mathbb{J}_3(\mathbf{u})\nabla_{\mathbf{u}} H$ is

$$\dot{\mathbf{p}}_a = \left(\frac{p_{a,2}B_{3,h}^{n+1}(\mathbf{x}_a)}{\gamma(\mathbf{p}_a, A_{3,h}^{n+1}(\mathbf{x}_a^n))}, -\frac{p_{a,1}B_3^{n+1}(\mathbf{x}_a)}{\gamma(\mathbf{p}_a, A_{3,h}^{n+1}(\mathbf{x}_a^n))}\right)^\top, \quad \dot{\mathbf{s}}_a = \mathbf{s}_a \times \mathbf{B}_h^{n+1}(\mathbf{x}_a), \quad 0 \le a < N_p. \tag{34}$$

As $|\mathbf{p}_a|^2$ is conserved by this subsystem, the velocity and spin variables can be solved exactly using Rodrigues' formula as (27), and naturally energy is conserved. The solution map from n-th to $(n+1)$-th time step is denoted as $\Phi^n_{ps}(\Delta t)$.

Subsystem IV The final subsystem $\dot{\mathbf{u}} = \mathbb{J}_4(\mathbf{u})\nabla_{\mathbf{u}} H$ about $\mathbf{x}_a, \mathbf{p}_a, \mathbf{e}_{12}$ is

$$\begin{aligned}&\dot{\mathbf{x}}_a = \frac{\mathbf{p}_a}{\sqrt{1 + |\mathbf{p}_a|^2 + |A_z(\mathbf{x}_a)|^2}},\\ &\dot{\mathbf{p}}_a = \mathbf{E}_{12,h}(\mathbf{x}_a) - \frac{A_{3,h}(\mathbf{x}_a)\nabla_{\mathbf{x}} A_{3,h}(\mathbf{x}_a)}{\gamma(\mathbf{p}_a, A_{z,h}(\mathbf{x}_a))},\\ &-\hbar s_x^a \left(\partial^2_{x_1x_2}A_3(\mathbf{x}_a), \partial^2_{x_2}A_3(\mathbf{x}_a)\right)^\top + \hbar s_2^a \left(\partial^2_{x_1}A_3(\mathbf{x}_a), \partial^2_{x_1x_2}A_3(\mathbf{x}_a)\right)^\top - \hbar s_3^a \left(\partial_{x_1}B_3(\mathbf{x}_a), \partial_{x_2}B_3(\mathbf{x}_a)\right)^\top,\\ &\dot{\mathbf{e}}_{12} = -\mathbb{M}_1^{-1}\sum_{a=1}^{N_p}\Lambda_1(\mathbf{x}_a)w_a\frac{\mathbf{p}_a}{\gamma(\mathbf{p}_a, A_{3,h}(\mathbf{x}_a))}.\end{aligned} \tag{35}$$

With the discrete gradients about $\mathbf{x}_a, \mathbf{p}_a, \mathbf{e}_{12}$,

$$\bar{\nabla}_{\mathbf{x}_a} H = w_a \frac{\left(A_{3,h}^{n+1}(\mathbf{x}_a^{n+1}) + A_{3,h}^{n+1}(\mathbf{x}_a^n)\right) \cdot \left(\frac{A_{3,h}^{n+1}(x_{1,a}^{n+1}, x_{2,a}^{n+1}) - A_{3,h}^{n+1}(x_{1,a}^n, x_{2,a}^{n+1})}{(x_{1,a}^{n+1} - x_{1,a}^n)}, \frac{A_{3,h}^{n+1}(x_{1,a}^n, x_{2,a}^{n+1}) - A_{3,h}^{n+1}(x_{1,a}^n, x_{2,a}^n)}{(x_{2,a}^{n+1} - x_{2,a}^n)}\right)^\top}{\sqrt{1 + |\mathbf{p}_a^n|^2 + |A_{3,h}^{n+1}(\mathbf{x}_a^{n+1})|^2} + \sqrt{1 + |\mathbf{p}_a^n|^2 + |A_{3,h}^{n+1}(\mathbf{x}_a^n)|^2}},$$

$$+ w_a \hbar s_{a,x}^{n+1} \left(\frac{\partial_y A_{3,h}^{n+1}(x_{1,a}^{n+1}, x_{2,a}^{n+1}) - \partial_y A_{3,h}^{n+1}(x_{1,a}^n, x_{2,a}^{n+1})}{x_{1,a}^{n+1} - x_{1,a}^n}, \frac{\partial_y A_{3,h}^{n+1}(x_{1,a}^n, x_{2,a}^{n+1}) - \partial_y A_{3,h}^{n+1}(x_{1,a}^n, x_{2,a}^n)}{x_{2,a}^{n+1} - x_{2,a}^n}\right)^\top,$$

$$- w_a \hbar s_{a,y}^{n+1} \left(\frac{\partial_x A_{3,h}^{n+1}(x_{1,a}^{n+1}, x_{2,a}^{n+1}) - \partial_x A_{3,h}^{n+1}(x_{1,a}^n, x_{2,a}^{n+1})}{x_{1,a}^{n+1} - x_{1,a}^n}, \frac{\partial_x A_{3,h}^{n+1}(x_{1,a}^n, x_{2,a}^{n+1}) - \partial_x A_{3,h}^{n+1}(x_{1,a}^n, x_{2,a}^n)}{x_{2,a}^{n+1} - x_{2,a}^n}\right)^\top,$$

$$+ w_a \hbar s_{a,z}^{n+1} \left(\frac{B_{3,h}^{n+1}(x_{1,a}^{n+1}, x_{2,a}^{n+1}) - B_{3,h}^{n+1}(x_{1,a}^n, x_{2,a}^{n+1})}{x_{1,a}^{n+1} - x_{1,a}^n}, \frac{B_{3,h}^{n+1}(x_{1,a}^n, x_{2,a}^{n+1}) - B_{3,h}^{n+1}(x_{1,a}^n, x_{2,a}^n)}{x_{2,a}^{n+1} - x_{2,a}^n}\right)^\top,$$

$$\bar{\nabla}_{\mathbf{p}_a} H = w_a \frac{\mathbf{p}_a^n + \mathbf{p}_a^{n+1}}{\gamma(\mathbf{p}_a^n, A_{3,h}^n(\mathbf{x}_a^{n+1})) + \gamma(\mathbf{p}_a^{n+1}, A_{3,h}^n(\mathbf{x}_a^{n+1}))}, \quad \bar{\nabla}_{\mathbf{e}_{12}} H = \mathbb{M}_1 \mathbf{e}_{12}^{n+\frac{1}{2}},$$

we have the following scheme,

$$\frac{\mathbf{x}_a^{n+1} - \mathbf{x}_a^n}{\Delta t} = \frac{\mathbf{p}_a^n + \mathbf{p}_a^{n+1}}{\gamma(\mathbf{p}_a^n, A_{3,h}^{n+1}(\mathbf{x}_a^{n+1})) + \gamma(\mathbf{p}_a^{n+1}, A_{3,h}^{n+1}(\mathbf{x}_a^{n+1}))},$$

$$\frac{\mathbf{p}_a^{n+1} - \mathbf{p}_a^n}{\Delta t} = \frac{1}{\Delta t} \int_{t^n}^{t^{n+1}} (\mathbf{\Lambda}^1(\mathbf{x}_a(\tau)))^\top \mathrm{d}\tau \mathbf{e}_{12}^{n+\frac{1}{2}} - \frac{1}{w_a} \bar{\nabla}_{\mathbf{x}_a} H,$$

$$\frac{\mathbf{e}_{12}^{n+1} - \mathbf{e}_{12}^n}{\Delta t} = -\mathbb{M}_1^{-1} \sum_{a=0}^{N_p-1} \frac{1}{\Delta t} \int_{t^n}^{t^{n+1}} \mathbf{\Lambda}^1(\mathbf{x}_a(\tau)) \mathrm{d}\tau w_a \frac{\mathbf{p}_a^n + \mathbf{p}_a^{n+1}}{\gamma(\mathbf{p}_a^n, A_{3,h}^{n+1}(\mathbf{x}_a^{n+1})) + \gamma(\mathbf{p}_a^{n+1}, A_{3,h}^{n+1}(\mathbf{x}_a^{n+1}))}.$$

where the time-continuous trajectory is defined as

$$\mathbf{x}_a(\tau) = \mathbf{x}_a^n + (\tau - t^n) \frac{\mathbf{x}_a^{n+1} - \mathbf{x}_a^n}{\Delta t}, \quad \tau \in [t^n, t^{n+1}], \quad 0 \le a < N_p.$$

Similar to remark 2, we can also prove discrete Poisson equation is satisfied by the numerical solution. The solution map from n-th to $(n+1)$-th time step is denoted as $\Phi_{xpe12}^n(\Delta t)$.

Then using the Lie splitting [17] gives us the first order approximate solution of (23),

$$\Phi(\mathbf{u}^n) = \Phi_{xpe12}^n(\Delta t) \Phi_{ps}^n(\Delta t) \Phi_{e12b3}^n(\Delta t) \Phi_{e3a3}^n(\Delta t) \mathbf{u}^n. \tag{36}$$

4.3 Higher order discrete gradient methods

Other discrete gradients such as second order average vector field methods [37], and midpoint discrete gradient [14] can also be chosen. For our models (16) and (23), since there are square root functions in the Hamiltonians (15) and (22), the average vector field methods require sufficient quadrature points to conserve the energies at the levels of quadrature errors (not exactly) as in [42]. In the following we apply the second order midpoint discrete gradient [14] to the above two dimensional system (23) as an example. One dimensional system (16) can be discretized in time in a similar way.

For the conservative equation (24), midpoint discrete gradient is

$$\bar{\nabla}H(\mathbf{u}^n,\mathbf{u}^{n+1})=\nabla H\left(\frac{\mathbf{u}^n+\mathbf{u}^{n+1}}{2}\right)+\frac{H(\mathbf{u}^{n+1})-H(\mathbf{u}^n)-\nabla H(\frac{\mathbf{u}^n+\mathbf{u}^{n+1}}{2})\cdot(\mathbf{u}^{n+1}-\mathbf{u}^n)}{|\mathbf{u}^{n+1}-\mathbf{u}^n|^2}\left(\mathbf{u}^{n+1}-\mathbf{u}^n\right). \tag{37}$$

When applying midpoint discrete gradient to (23) directly, all components of $\mathbf{u}$ are coupled by some nonlinear terms due to the square root function in Hamiltonian (22) and the term $|\mathbf{u}^{n+1}-\mathbf{u}^n|^2$ in (37), thus the nonlinear iterations are needed. However, using midpoint discrete gradient to the four subsystems (29), (31), (34), and (35) after Poisson splitting makes the computations more efficient. Next we present the discretizations of two subsystems (29) and (35).

Subsystem I The midpoint discrete gradients about $(\mathbf{e}_3,\mathbf{a}_3)$ are

$$\begin{aligned}\bar{\nabla}\mathbf{e}_3H&=\mathbb{M}_0\mathbf{e}_3^{n+\frac{1}{2}}+C_{ea}(\mathbf{e}_3^{n+1}-\mathbf{e}_3^n),\\ \bar{\nabla}\mathbf{a}_3H&=\nabla_{\mathbf{a}_3}H(\mathbf{a}_3^{n+\frac{1}{2}})+C_{ea}(\mathbf{a}_3^{n+1}-\mathbf{a}_3^n),\end{aligned}$$

where $C_{ea}=\frac{H(\mathbf{e}_3^{n+1},\mathbf{a}_3^{n+1})-H(\mathbf{e}_3^n,\mathbf{a}_3^n)-\nabla_{\mathbf{e}_3}H(\frac{\mathbf{e}_3^n+\mathbf{e}_3^{n+1}}{2})\cdot(\mathbf{e}_3^{n+1}-\mathbf{e}_3^n)-\nabla_{\mathbf{a}_3}H(\frac{\mathbf{a}_3^n+\mathbf{a}_3^{n+1}}{2})\cdot(\mathbf{a}_3^{n+1}-\mathbf{a}_3^n)}{|\mathbf{e}_3^{n+1}-\mathbf{e}_3^n|^2+|\mathbf{a}_3^{n+1}-\mathbf{a}_3^n|^2}$. Then we have the following scheme,

$$\frac{\mathbf{a}_3^{n+1}-\mathbf{a}_3^n}{\Delta t}=-\mathbb{M}_0^{-1}\bar{\nabla}_{\mathbf{e}_3}H,\quad \frac{\mathbf{e}_3^{n+1}-\mathbf{e}_3^n}{\Delta t}=\mathbb{M}_0^{-1}\bar{\nabla}_{\mathbf{a}_3}H.$$

The solution map from n-th to $(n+1)$-th time step is denoted as $\Phi_{e3a3}^{n,mid}(\Delta t)$.

Subsystem II As Hamiltonian (22) depends on $\mathbf{e}_{12},\mathbf{b}_3$ quadratically, the scheme by using midpoint discrete gradient is the same as (32).

Subsystem III This subsystem is the same as (34) which can be solved analytically.

Subsystem IV The midpoint discrete gradients about $(\mathbf{X},\mathbf{P},\mathbf{e}_{12})$ are

$$\begin{aligned}\bar{\nabla}\mathbf{x}_aH&=\nabla_{\mathbf{x}_a}H(\mathbf{x}_a^{n+\frac{1}{2}},\mathbf{p}_a^{n+\frac{1}{2}})+C_{xpe}(\mathbf{x}_a^{n+1}-\mathbf{x}_a^n),\\ \bar{\nabla}\mathbf{p}_aH&=\nabla_{\mathbf{p}_a}H(\mathbf{x}_a^{n+\frac{1}{2}},\mathbf{p}_a^{n+\frac{1}{2}})+C_{xpe}(\mathbf{p}_a^{n+1}-\mathbf{p}_a^n),\\ \bar{\nabla}\mathbf{e}_{12}H&=\mathbb{M}_1\mathbf{e}_{12}^{n+\frac{1}{2}}+C_{xpe}(\mathbf{e}_{12}^{n+1}-\mathbf{e}_{12}^n),\end{aligned}$$

where $C_{xpe}=\frac{H(\mathbf{X}^{n+1},\mathbf{P}^{n+1},\mathbf{e}_{12}^{n+1})-H(\mathbf{X}^n,\mathbf{P}^n,\mathbf{e}_{12}^n)-\nabla_{\mathbf{XP}}H(\frac{\mathbf{X}^n+\mathbf{X}^{n+1}}{2},\frac{\mathbf{P}^n+\mathbf{P}^{n+1}}{2})\cdot(\mathbf{X}^{n+1}-\mathbf{X}^n,\mathbf{P}^{n+1}-\mathbf{P}^n)}{|\mathbf{X}^{n+1}-\mathbf{X}^n|^2+|\mathbf{P}^{n+1}-\mathbf{P}^n|^2+|\mathbf{e}_{12}^{n+1}-\mathbf{e}_{12}^n|^2}$. Then we have the following scheme,

$$\begin{aligned}\frac{\mathbf{x}_a^{n+1}-\mathbf{x}_a^n}{\Delta t}&=\frac{1}{w_a}\bar{\nabla}\mathbf{p}_aH,\\ \frac{\mathbf{p}_a^{n+1}-\mathbf{p}_a^n}{\Delta t}&=\frac{1}{\Delta t}\int_{t^n}^{t^{n+1}}(\mathbf{\Lambda}^1(\mathbf{x}_a(\tau))^\top\mathrm{d}\tau\bar{\nabla}\mathbf{e}_{12}H-\frac{1}{w_a}\bar{\nabla}_{\mathbf{x}_a}H,\\ \frac{\mathbf{e}_{12}^{n+1}-\mathbf{e}_{12}^n}{\Delta t}&=-\mathbb{M}_1^{-1}\sum_{a=0}^{N_p-1}\frac{1}{\Delta t}\int_{t^n}^{t^{n+1}}\mathbf{\Lambda}^1(\mathbf{x}_a(\tau)\mathrm{d}\tau\bar{\nabla}\mathbf{p}_aH,\end{aligned}$$

where the time-continuous trajectory is defined as

$$\mathbf{x}_a(\tau)=\mathbf{x}_a^n+(\tau-t^n)\frac{\mathbf{x}_a^{n+1}-\mathbf{x}_a^n}{\Delta t},\quad \tau\in[t^n,t^{n+1}],\quad 1\le a<N_p.$$

The solution map from n-th to $(n+1)$-th time step is denoted as $\Phi^{n,mid}_{xpe12}(\Delta t)$.

Finally using Strang splitting [17] gives the second order accuracy in time,

$$\Phi(\mathbf{u}^n) = \Phi^{n,mid}_{xpe12}(\frac{\Delta t}{2})\Phi^n_{ps}(\frac{\Delta t}{2})\Phi^n_{e12b3}(\frac{\Delta t}{2})\Phi^{n,mid}_{e3a3}(\Delta t)\Phi^n_{e12b3}(\frac{\Delta t}{2})\Phi^n_{ps}(\frac{\Delta t}{2})\Phi^{n,mid}_{xpe12}(\frac{\Delta t}{2})\mathbf{u}^n. \quad (38)$$

5 Numerical experiments

In this section, we firstly check the time accuracy orders of the first and second order discrete gradient methods and the performances of the pre-conditioners mentioned in section 4. Then some numerical experiments are conducted for one and two dimensional relativistic Vlasov–Maxwell systems. In both cases, energy errors are at the level of iteration tolerances, also we verify that discrete Poisson equations are satisfied by the numerical solutions numerically. Moreover, numerical growth rates of some Fourier modes and numerical dispersion relations are compared with the analytical results. Some contour plots of the distribution functions are shown to illustrate the vortex structures appeared in the processes of laser plasma interactions.

5.1 Accuracy and performance

As for the time accuracy, we check the convergence results of the first and second order discrete gradient methods (36) and (38) for the two dimensional case. Reference solutions are obtained by using sufficiently small step sizes. We can see that in Table. 1 and 2, the convergence orders of particle related energy, electric energy, and magnetic energy are all around one and two, respectively. As for the performances of pre-conditioners, we compare the iteration numbers needed for solving the linear systems (25), (30), and (33) of the cases with and without pre-conditioners, in which the same randomly generated right hand values are used. The results of comparisons are listed in Table. 3, we find that the pre-conditioners are quite efficient and robust.

Δt	particle related energy (order)	electric energy (order)	magnetic energy (order)
0.001	2.60×10^{-5}	1.85×10^{-7}	2.58×10^{-5}
0.0005	1.29×10^{-5} (1.01)	6.95×10^{-8} (1.22)	1.28×10^{-5}(1.01)
0.00025	6.38×10^{-6} (1.01)	2.88×10^{-8}(1.22)	6.36×10^{-6} (1.01)
0.000125	3.13×10^{-6} (1.02)	1.27×10^{-8} (1.13)	3.11×10^{-6} (1.02)

Table 1: **Time accuracy order**: first order discrete gradient method (36).

Δt	particle related energy (order)	electric energy (order)	magnetic energy (order)
0.01	4.32×10^{-3}	4.02×10^{-3}	2.98×10^{-4}
0.005	1.11×10^{-3} (1.95)	1.03×10^{-3} (1.95)	7.7×10^{-5} (1.94)
0.0025	2.77×10^{-4} (2.00)	2.58×10^{-4} (2.00)	1.94×10^{-5} (1.98)
0.00125	6.86×10^{-5} (2.19)	6.38×10^{-5} (2.02)	4.79×10^{-6} (2.03)
0.000625	1.63×10^{-6} (2.10)	1.52×10^{-5} (2.10)	1.14×0^{-6} (2.10)

Table 2: **Time accuracy order**: second order discrete gradient method (38).

Equations	with pre-conditioner	without pre-conditioner
(25)	7	56
(30)	7	228
(33)	7	202

Table 3: **Performances of pre-conditioners**: time step size is $\Delta t = 0.01$, one dimensional grids are 128, two dimensional grids are 128×64.

5.2 One dimensional test

For this one dimensional model, we conduct the so-called parametric instability [5] without and with spin effects. The initial distribution function is chosen as a homogeneous Maxwellian with low temperature expressed as

$$f_0(x,p) = \frac{1}{\sqrt{2\pi T}} \exp\left(-\frac{p^2}{2T}\right), \quad T = 3/511. \tag{39}$$

Initial consistent electrostatic electric field, i.e., E_1 is $E_{1,0}(x) = 0$. Scaled Planck constant is set as 0. Initially, the laser in transverse directions is

$$E_{2,0}(x) = -E_0 \cos(kx), E_{3,0}(x) = -E_0 \sin(kx), A_{2,0}(x) = -E_0 \sin(kx), A_{3,0}(x) = E_0 \cos(kx), \tag{40}$$

with a wavenumber $k = 1/\sqrt{2}$ and amplitude $E_0 = \sqrt{3}$, from which we can calculate out the time frequency ω_0 of the laser equals 1 by the dimensionless dispersion relation $\omega_0^2 = \sqrt{\frac{1}{\sqrt{1+E_0^2}} + k^2}$ [6]. The domain of the simulation is $[0, \frac{2\pi}{k}]$, time step size is $\Delta t = 0.02$, cell number in space is 128, total particle number is 10^5, the degree of B-spline in (10) is 3, and Lie–Trotter splitting (28) is used, and iteration tolerances are set as 10^{-12}.

The time evolutions of relative energy error and Poisson equation error are plotted in Fig. 1. We can see that both the errors are very small, and have no obvious growth with time. In Fig. 2, we compare the numerical growth rates of the second Fourier mode of E_1 and E_2 with analytical rates (red lines) [5], which fit in well and validate the code. We also plot the contour plots of distribution functions at time $t = 10, 40$ in Fig. 3, and there are two vortex structures due to the laser plasma interactions and particle trapping.

In order to check the dispersion relation $\omega^2 = \sqrt{\frac{1}{\sqrt{1+E_0^2}} + k^2}$ of circularly polarized electromagnetic waves numerically, we use the following initial values of electromagnetic fields in transverse direction, i.e.,

$$E_{2,0}(x) = -E_0 \sum_{i=1}^{6} \cos(ikx), E_{3,0}(x) = -E_0 \sum_{i=1}^{6} \sin(ikx), A_{2,0}(x) = -E_0 \sum_{i=1}^{6} \sin(ikx), A_{3,0}(x) = E_0 \sum_{i=1}^{6} \cos(ikx).$$

The numerical and analytical dispersion relations are quite close, which are presented in Fig. 4.

Next we include spin effects by setting $\mathfrak{h} = 0.1$. The same computational parameters and initial conditions for the fields (40) are chosen, but a different initial distribution function is used, i.e.,

$$f_0(x,p,\mathbf{s}) = \frac{1}{\sqrt{2\pi T}} \exp(-\frac{p^2}{2T})\delta(\mathbf{s} - (0,0,1)^\top), \quad T = 3/511.$$

We can see that the spin vectors of all the particles are pointing at the $(0,0,1)$ direction, i.e., there is a polarization for the spin in the plasmas initially. From Fig. 5, we see that the energy

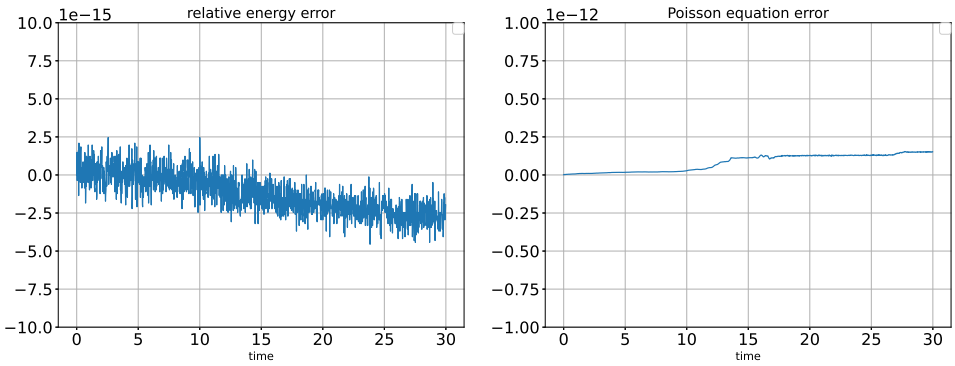

Figure 1: **1D without spin**: time evolutions of relative energy error and poisson equation error.

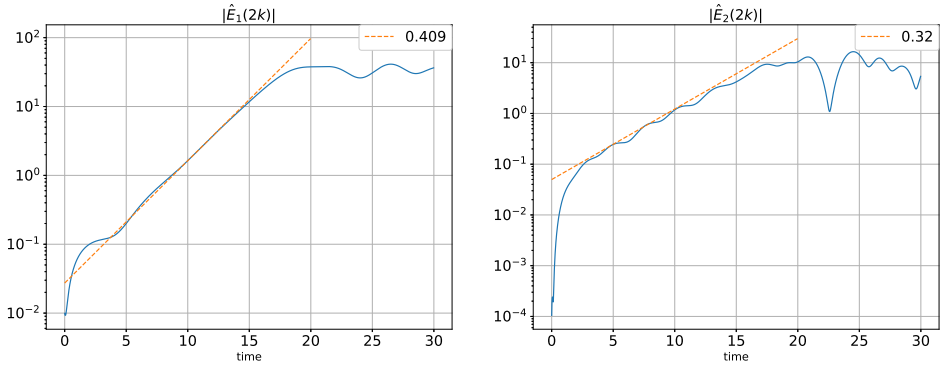

Figure 2: **1D without spin**: time evolutions of the amplitudes of the second Fourier mode of E_1 and E_2.

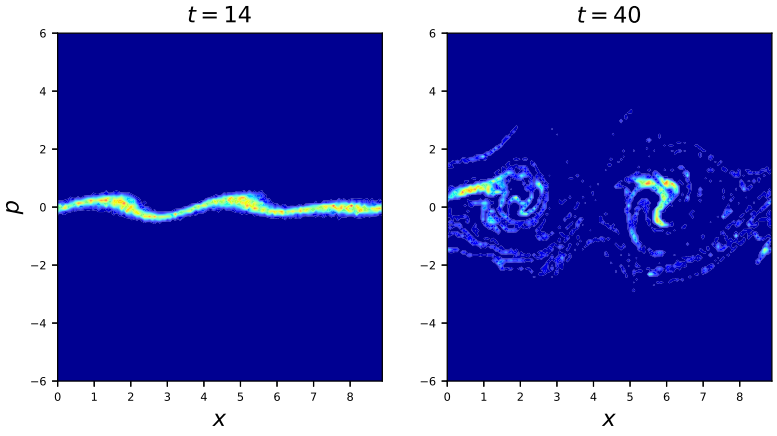

Figure 3: **1D without spin**: contour plots of (x, p) at $t = 10, 40$.

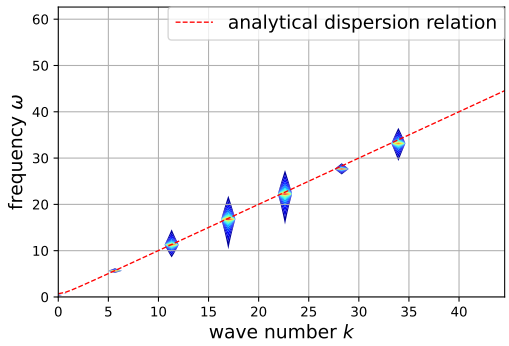

Figure 4: **1D without spin**: comparison of numerical dispersion relation with analytical one.

error and poisson equation error are quite small and have no obvious growth with time. In Fig. 6, time evolutions of spin momentum $S_y = \int s_2 f \mathrm{d}\mathbf{s}\mathrm{d}p\mathrm{d}x$ and $S_z = \int s_3 f \mathrm{d}\mathbf{s}\mathrm{d}p\mathrm{d}x$ at y and z directions are plotted, we find that the momenta oscillate with time and decay to zero finally, which are similar to the results of non-relativistic case in [4]. The oscillatory behavior can be explained approximately from the equations of spin vector of each particle $\dot{\mathbf{s}} = \mathbf{s} \times \mathbf{B}$. The reason of the decays of S_y and S_z in Fig. 6 is that the polarization of spin are destroyed by a combination of thermal effects and the parametric instability (including Raman instability) [4].

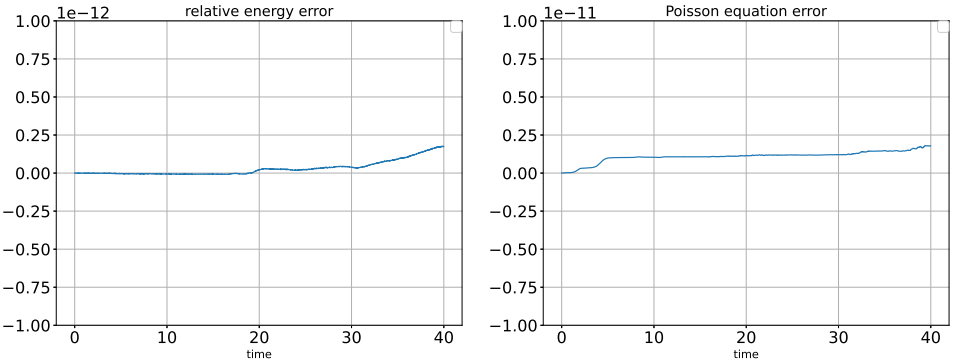

Figure 5: **1D with spin**: time evolutions of relative energy error and poisson equation error.

5.3 Two dimensional test

For the two dimensional system, we choose the following initial condition,

$$f_0(\mathbf{x}, \mathbf{p}) = \frac{1}{\pi v_T^2} \exp\left(-\frac{p_1^2}{v_T^2}\right) \exp\left(-\frac{|p_2 + A_2(\mathbf{x})|^2}{v_T^2}\right),$$

where $\mathbf{E}(\mathbf{x}) = (0, E_0 \cos(k_0 x_1), E_0 \sin(k_0 x_1))$, $A_3(\mathbf{x}) = -\frac{E_0}{\omega_0} \cos(k_0 x_1)$, $A_2(\mathbf{x}) = \frac{E_0}{\omega_0} \sin(k_0 x_1)$, $B_3(\mathbf{x}) = \frac{k_0}{\omega_0} E_0 \cos(k_0 x_1)$, $k_0 = \sqrt{\frac{3}{2}}$, domain is $[0, \frac{2\pi}{k_x}] \times [0, \frac{2\pi}{k_y}]$, $v_T^2 = 0.001$, $k_x = 0.6125$, $k_y = 0.866$, $\omega_0 = \sqrt{2}$, $E_0 = \sqrt{3}$, and $\mathfrak{h} = 0$. Cell number is 256×128, total particle number

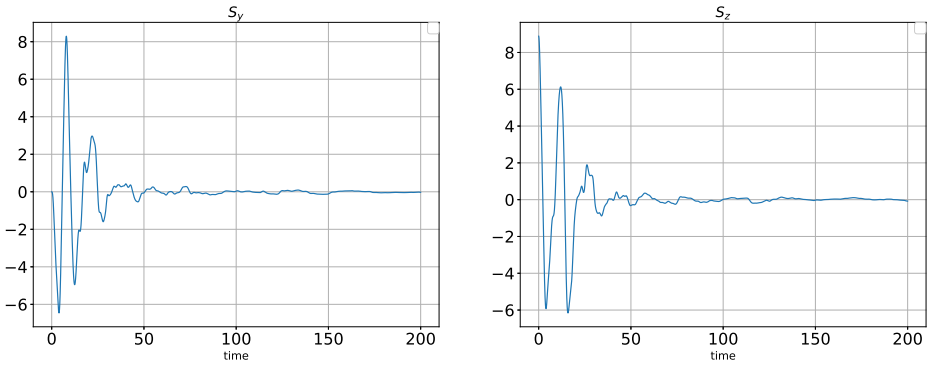

Figure 6: **1D with spin**: time evolutions of $S_y = \int s_2 f \mathrm{d}\mathbf{s}\mathrm{d}p\mathrm{d}x$ and $S_z = \int s_3 f \mathrm{d}\mathbf{s}\mathrm{d}p\mathrm{d}x$.

is 4×10^6, time step size is 0.01, the degrees of B-spline in (17) is $(2, 2)$, Lie splitting (36) is used, and iteration tolerances are set as 10^{-10}. The implementaion of the 2D test is done in the python package [32].

We plot the time evolutions of some Fourier modes in Fig. 7, which are consistent with the analytical results (red dash lines) as [6]. Unstable Fourier modes predicted from the the linear theory grow with time exponentially. As mentioned in [6], all modes involved in the parametric instabilities are in a mixed polarization state.

The errors of energy and Poisson equation (difference from the initial error) are presented in Fig. 8, which validate the conservation properties of the numerical schemes. The sufficient particle number (4×10^6) enables us to get very fine resolutions and mechanisms in phase space. The contour plots of (x_1, p_1) and (x_1, p_2) are plotted in Fig. 9. As the domain size in x_1 direction is two times of the wavelength of the laser injected into the plasma, there are four vortex structures in (x_1, p_1) contour plots due to particle trapping in plasma waves. The modulation in the (x_1, p_2) contour plots is due to the introduction of the A_2 shift in the initial distribution function.

To include spin effects, we set $\hbar = 0.1$, and degrees of B-splines in (17) are $(3, 3)$, total particle number is 4×10^5. The initial conditions and computational parameters are the same as the case above without spin effect, except that the initial distribution function is

$$f_0(\mathbf{x}, \mathbf{p}) = \frac{1}{\pi v_T^2} \exp\left(-\frac{p_1^2}{v_T^2}\right) \exp\left(-\frac{|p_2 + A_2(\mathbf{x})|^2}{v_T^2}\right) \delta(\mathbf{s} - (0, 0, 1)^\top).$$

In Fig. 10, the time evolutions of momentums about $\mathbf{s}$ are plotted, we can see that as the one dimensional case, the momentums oscillate and decay with time. The errors of energy and Poisson equation (difference from the initial error) are displayed in Fig. 11, which are both at the level of iteration tolerance.

6 Conclusion

In this work, discrete gradients are used to construct energy conserving particle-in-cell schemes for one and two dimensional relativistic Vlasov–Maxwell equations with spin effects. The space discretization of fields is done in the framework of finite element exterior calculus. Numerical experiments are conducted to validate our numerical schemes, especially the conservation properties. Three dimensional case is not detailed in this work, as the relativistic factor $\sqrt{1 + |\mathbf{p}|^2}$

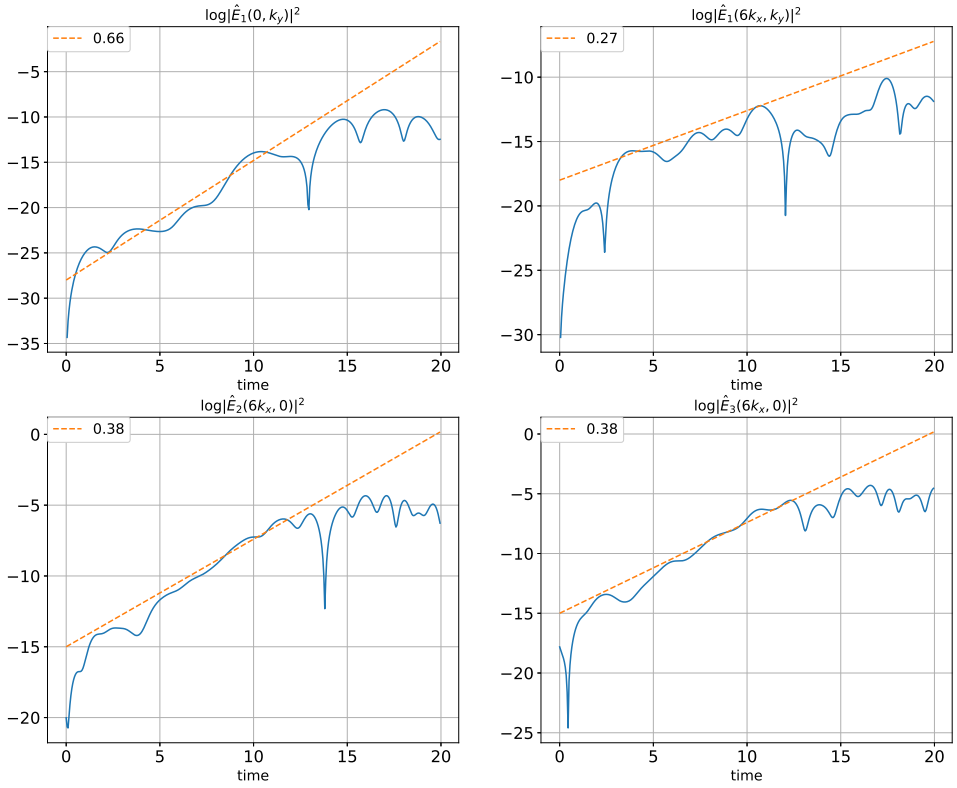

Figure 7: **2D without spin**: time evolutions of Fourier modes of the components of the electric field.

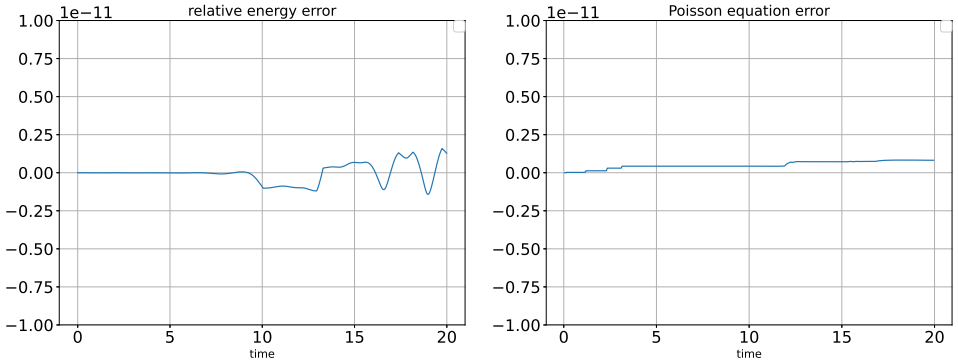

Figure 8: **2D without spin**: time evolutions of relative energy error and Poisson equation error.

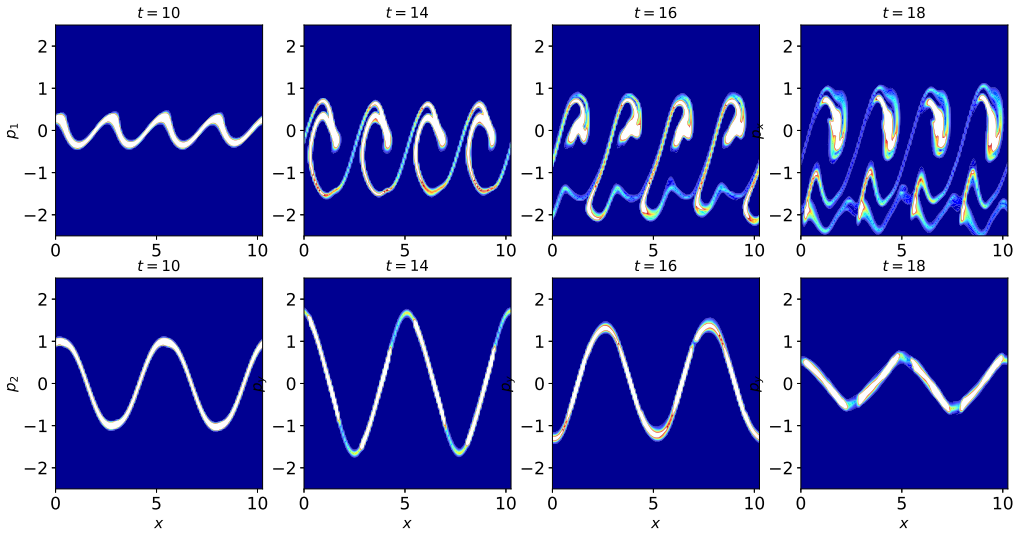

Figure 9: **2D without spin**: contour plots of (x_1, p_1) and (x_1, p_2) at $t = 10, 14, 16, 18$.

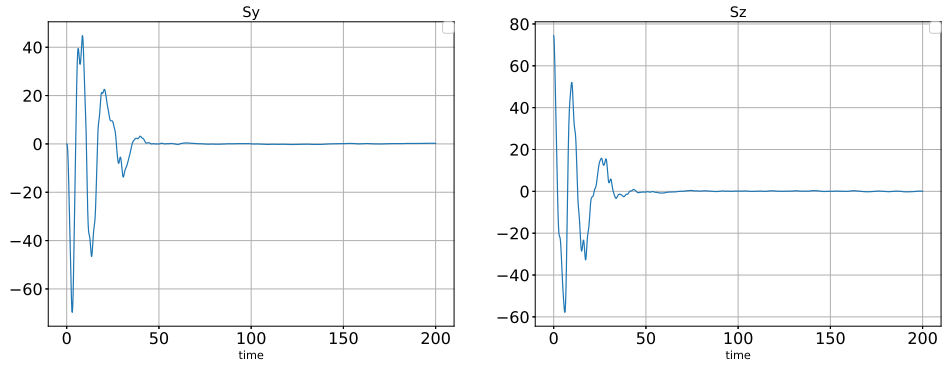

Figure 10: **2D with spin**: time evolutions of $S_y = \int s_2 f \mathrm{d}\mathbf{s}\mathrm{d}\mathbf{p}\mathrm{d}\mathbf{x}$ and $S_z = \int s_3 f \mathrm{d}\mathbf{s}\mathrm{d}\mathbf{p}\mathrm{d}\mathbf{x}$.

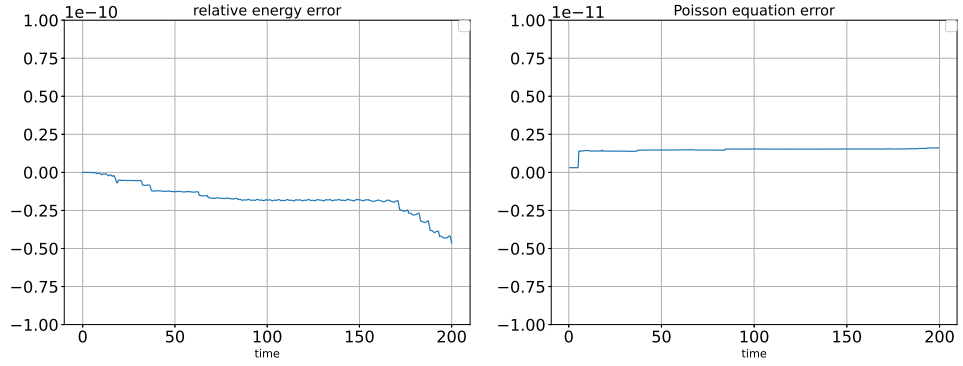

Figure 11: **2D with spin**: time evolutions of relative energy error and Poisson equation error.

does not depends on particle position, and thus is easier to apply the discrete gradient methods. There are several future works to be envisaged, such as parallelization of the code, implementation of non-periodic boundary condition as [24], and so on.

7 Appendix

7.1 Discrete functional derivatives of 2D reduced model

$$\frac{\delta \mathcal{F}}{\delta E_3} = (\mathbf{\Lambda}^0)^\top \mathbb{M}_0^{-1} \nabla_{\mathbf{e}_3} F, \quad \frac{\delta \mathcal{F}}{\delta A_3} = (\mathbf{\Lambda}^0)^\top \mathbb{M}_0^{-1} \nabla_{\mathbf{a}_3} F,$$
$$\frac{\delta \mathcal{F}}{\delta \mathbf{E}_{12}} = (\mathbf{\Lambda}^1)^\top \mathbb{M}_1^{-1} \nabla_{\mathbf{e}_{12}} F, \quad \frac{\delta \mathcal{F}}{\delta B_3} = (\mathbf{\Lambda}^2)^\top \mathbb{M}_2^{-1} \nabla_{\mathbf{b}_3} F,$$
$$\frac{\partial}{\partial \mathbf{x}} \frac{\delta \mathcal{F}}{\delta f} | (\mathbf{x}_a, \mathbf{p}_a, \mathbf{s}_a) = \frac{1}{w_a} \nabla_{\mathbf{x}_a} F, \quad \frac{\partial}{\partial \mathbf{p}} \frac{\delta \mathcal{F}}{\delta f} | (\mathbf{x}_a, \mathbf{p}_a, \mathbf{s}_a) = \frac{1}{w_a} \nabla_{\mathbf{p}_a} F, \frac{\partial}{\partial \mathbf{s}} \frac{\delta \mathcal{F}}{\delta f} | (\mathbf{x}_a, \mathbf{p}_a, \mathbf{s}_a) = \frac{1}{w_a} \nabla_{\mathbf{s}_a} F. \tag{41}$$

References

[1] Sheng Z M, Mima K, Sentoku Y, Jovanović M S, Taguchi T, Zhang J, Meyer-ter-Vehn J. Stochastic heating and acceleration of electrons in colliding laser fields in plasma. Physical review letters, 2002, 88(5): 055004.

[2] Li Y, Sun Y, Crouseilles N. Numerical simulations of one laser-plasma model based on Poisson structure. Journal of Computational Physics, 2020, 405, 109172.

[3] Marklund M, Morrison P J. Gauge-free Hamiltonian structure of the spin Maxwell–Vlasov equations. Physics Letters A, 2011, 375(24), 2362-2365.

[4] Crouseilles N, Hervieux P A, Li Y, Manfredi G, Sun Y. Geometric particle-in-cell methods for the Vlasov–Maxwell equations with spin effects. Journal of Plasma Physics, 2021, 87(3).

[5] Ghizzo A, Bertrand P, Shoucri M M, et al. A Vlasov code for the numerical simulation of stimulated Raman scattering. Journal of Computational Physics, 1990, 90(2): 431-457.

[6] Bégué M L, Ghizzo A, Bertrand P, et al. Two-dimensional semi-Lagrangian Vlasov simulations of laser-plasma interaction in the relativistic regime. Journal of plasma physics, 1999, 62(4): 367-388.

[7] Bostan M. Mild solutions for the relativistic Vlasov-Maxwell system for laser-plasma interaction. Quarterly of applied mathematics, 2007, 65(1): 163-187.

[8] Carrillo J A, Labrunie S. Global solutions for the one-dimensional Vlasov–Maxwell system for laser-plasma interaction. Mathematical Models and Methods in Applied Sciences, 2006, 16(01): 19-57.

[9] Bostan M, Crouseilles N. Convergence of a semi-Lagrangian scheme for the reduced Vlasov–Maxwell system for laser-plasma interaction. Numerische Mathematik, 2009, 112(2): 169-195.

[10] Cheng Y, Christlieb A J, Zhong X. Energy-conserving discontinuous Galerkin methods for the Vlasov–Ampère system. Journal of Computational Physics, 2014, 256: 630-655.

[11] Birdsall C K, Langdon A B. Plasma physics via computer simulation. CRC press, 2018.

[12] Hockney R W, Eastwood J W. Computer simulation using particles. CRC Press, 2021.

[13] Sonnendrücker E, Roche J, Bertrand P, Ghizzo A. The semi-Lagrangian method for the numerical resolution of the Vlasov equation. Journal of computational physics, 1999, 149(2), 201-220.

[14] Gonzalez O. Time integration and discrete Hamiltonian systems. Journal of Nonlinear Science, 1006, 6(5), 449-467.

[15] Arnold D, Falk R, Winther R. Finite element exterior calculus: from Hodge theory to numerical stability. Bulletin of the American mathematical society, 2010, 47(2), 281-354.

[16] Feng K, Qin M. Symplectic geometric algorithms for Hamiltonian systems. Berlin: Springer, 2010.

[17] Hairer E, Lubich C, Wanner G. Geometric Numerical Integration: Structure-Preserving Algorithms for Ordinary Differential Equations, vol. 31, Springer Science & Business Media, 2006.

[18] McLachlan R I, Quispel G R W, Robidoux N. Geometric integration using discrete gradients. Philosophical Transactions of the Royal Society of London. Series A: Mathematical, Physical and Engineering Sciences, 1999, 357(1754), 1021-1045.

[19] Xiao J, Qin H, Liu J, He Y, Zhang R, Sun Y. Explicit high-order non-canonical symplectic particle-in-cell algorithms for Vlasov–Maxwell systems. Physics of Plasmas, 2015, 22(11), 112504.

[20] He Y, Sun Y, Qin H, Liu J. Hamiltonian particle-in-cell methods for Vlasov–Maxwell equations. Physics of Plasmas, 2016, 23(9), 092108.

[21] He Y, Qin H, Sun Y, Xiao J, Zhang R, Liu J. Hamiltonian time integrators for Vlasov–Maxwell equations. Physics of Plasmas, 2015, 22(12), 124503.

[22] Xiao J, Liu J, Qin H, Yu Z. A variational multi-symplectic particle-in-cell algorithm with smoothing functions for the Vlasov-Maxwell system. Physics of Plasmas, 2013, 20(10), 102517.

[23] Kraus M, Kormann K, Morrison P J, and Sonnendrücker E. GEMPIC: geometric electromagnetic particle-in-cell methods. Journal of Plasma Physics, 2017, 83(4).

[24] Perse B, Kormann K, and Sonnendrücker E. Geometric Particle-in-Cell Simulations of the Vlasov–Maxwell System in Curvilinear Coordinates. SIAM Journal on Scientific Computing 43.1 2021: B194-B218.

[25] Morrison P J. Structure and structure-preserving algorithms for plasma physics. Physics of Plasmas, 2017, 24(5), 055502.

[26] Shen J, Xu J, Yang J. The scalar auxiliary variable (SAV) approach for gradient flows. Journal of Computational Physics, 2018, 353: 407-416.

[27] Kormann K, Sonnendrücker E. Energy-conserving time propagation for a structure-preserving particle-in-cell Vlasov–Maxwell solver. Journal of Computational Physics, 2020, 425: 109890.

[28] Campos Pinto M, Kormann K, Sonnendrücker E. Variational framework for structure-preserving electromagnetic particle-in-cell methods. Journal of Scientific Computing, 2022, 91(2): 1-39.

[29] Buffa A, Sangalli G, Vázquez R. Isogeometric analysis in electromagnetics: B-splines approximation. Computer Methods in Applied Mechanics and Engineering, 2010, 199(17-20): 1143-1152.

[30] Crouseilles N, Einkemmer L, Faou E. Hamiltonian splitting for the Vlasov–Maxwell equations. Journal of Computational Physics, 2015, 283: 224-240.

[31] Wen M, Tamburini M, Keitel C H. Polarized laser-wakefield-accelerated kiloampere electron beams. Physical review letters, 2019, 122(21): 214801.

[32] Holderied F, Possanner S, Wang X. MHD-kinetic hybrid code based on structure-preserving finite elements with particles-in-cell. Journal of Computational Physics, 2021, 433: 110143.

[33] Hirani A N. Discrete exterior calculus. California Institute of Technology, 2003.

[34] Chen G, Chacón L, Yin L, et al. A semi-implicit, energy-and charge-conserving particle-in-cell algorithm for the relativistic Vlasov–Maxwell equations. Journal of Computational Physics, 2020, 407: 109228.

[35] Shiroto T, Ohnishi N, Sentoku Y. Quadratic conservative scheme for relativistic Vlasov–Maxwell system. Journal of Computational Physics, 2019, 379: 32-50.

[36] Itoh T, Abe K. Hamiltonian-conserving discrete canonical equations based on variational difference quotients. Journal of Computational Physics, 1988, 76(1): 85-102.

[37] Celledoni E, Grimm V, McLachlan R I, et al. Preserving energy resp. dissipation in numerical PDEs using the "Average Vector Field" method. Journal of Computational Physics, 2012, 231(20): 6770-6789.

[38] Yang H, Li F. Discontinuous Galerkin methods for relativistic Vlasov–Maxwell system. Journal of Scientific Computing, 2017, 73(2): 1216-1248.

[39] Marklund M, Zamanian J, Brodin G. Spin kinetic theory-quantum kinetic theory in extended phase space. Transport Theory and Statistical Physics, 2010, 39(5-7): 502-523.

[40] Asenjo F A, Zamanian J, Marklund M, et al. Semi-relativistic effects in spin-1/2 quantum plasmas. New Journal of Physics, 2012, 14(7): 073042.

[41] Zamanian J, Marklund M, Brodin G. Scalar quantum kinetic theory for spin-1/2 particles: mean field theory. New Journal of Physics, 2010, 12(4): 043019.

[42] Zhu B, Tang Y, Liu J. Energy-preserving methods for guiding center system based on averaged vector field. Physics of Plasmas, 2022, 29(3): 032501.

[43] Monk P. Finite element methods for Maxwell's equations. Oxford University Press, 2003.

[44] McLachlan R I, Quispel G R W, Robidoux N. Geometric integration using discrete gradients. Philosophical Transactions of the Royal Society of London. Series A: Mathematical, Physical and Engineering Sciences, 1999, 357(1754): 1021-1045.

[45] Lapenta G, Markidis S. Particle acceleration and energy conservation in particle in cell simulations. Physics of Plasmas, 2011, 18(7): 072101.